AD A062490

AFFDL-TR-78-121

ELECTROMAGNETIC COUPLING ANALYSIS OF A LEARJET AIRCRAFT

DR. D. F. STRAWE
M. O'BYRNE
S. SANDBERG

THE BOEING COMPANY
SEATTLE, WASHINGTON

SEPTEMBER 1978

TECHNICAL REPORT AFFDL-TR-78-121
Final Report — June 1977 - June 1978

Approved for public release; distribution unlimited.

AIR FORCE FLIGHT DYNAMICS LABORATORY
AIR FORCE WRIGHT AERONAUTICAL LABORATORIES
AIR FORCE SYSTEMS COMMAND
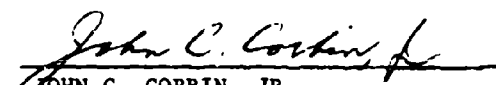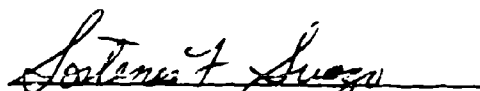WRIGHT-PATTERSON AIR FORCE BASE, OHIO 45433

78 12 11 041

JOHN C. CORBIN, JR.
Project Engineer

SOSTENES F. SUAZO, Lt Col, USAF
Chief, Survivability/Vulnerability Branch
Vehicle Equipment Division
AF Flight Dynamics Laboratory

FOR THE COMMANDER

AMBROSE B. NUTT
Director, Vehicle Equipment Division
AF Flight Dynamics Laboratory

REPORT DOCUMENTATION PAGE	READ INSTRUCTIONS BEFORE COMPLETING FORM

1. REPORT NUMBER	2. GOVT ACCESSION NO.	3. RECIPIENT'S CATALOG NUMBER
AFFDL-TR-78-121		

4. TITLE (and Subtitle)	5. TYPE OF REPORT & PERIOD COVERED
ELECTROMAGNETIC COUPLING ANALYSIS OF A LEARJET AIRCRAFT.	Final Report. 15 Jun 77 - 15 Jun 78.
	6. PERFORMING ORG. REPORT NUMBER
	D180-24256-1

7. AUTHOR(s)	8. CONTRACT OR GRANT NUMBER(s)
Dr. D. F. Strawe M. O'Byrne S. Sandberg	F33615-77-C-2058

9. PERFORMING ORGANIZATION NAME AND ADDRESS	10. PROGRAM ELEMENT, PROJECT, TASK AREA & WORK UNIT NUMBERS
The Boeing Company P. O. Box 3707 Seattle, Washington 98124	2402-02-01

11. CONTROLLING OFFICE NAME AND ADDRESS	12. REPORT DATE
Air Force Flight Dynamics Laboratory (FES) Air Force Systems Command Wright-Patterson AFB, Ohio 45433	Sep 1978
	13. NUMBER OF PAGES
	77

14. MONITORING AGENCY NAME & ADDRESS(If different from Controlling Office)	15. SECURITY CLASS. (of this report)
84p.	Unclassified
	15a. DECLASSIFICATION/DOWNGRADING SCHEDULE

16. DISTRIBUTION STATEMENT (of this Report)

Approved for public release; distribution unlimited.

17. DISTRIBUTION STATEMENT (of the abstract entered in Block 20, if different from Report)

18. SUPPLEMENTARY NOTES

19. KEY WORDS (Continue on reverse side if necessary and identify by block number)

EMP	TRAFFIC
Lightning	Learjet
WIRANT	

20. ABSTRACT (Continue on reverse side if necessary and identify by block number)

This report presents the results of an electromagnetic modeling analysis of a Learjet aircraft. Coupling models were developed for the aircraft exterior and selected internal cabling. Calculations of pulse induced responses were made using the computer codes WIRANT and TRAFFIC. The calculated responses were compared to test data obtained by AFFDL. Lightning-induced responses were also calculated for a nearby 20 kiloampere stroke.

DD FORM 1473 EDITION OF 1 NOV 65 IS OBSOLETE

PREFACE

This is the final report on the electromagnetic coupling analysis of the Learjet aircraft that was used for ground pulse tests and flight tests in a natural lightning environment at Kennedy Space Center in 1977. This analysis effort was performed for the Air Force Flight Dynamics Laboratory (AFFDL) under Contract F33615-77-C-2058.

AFFDL conducted the ground pulse tests and the flight tests. An analytical model developed for the Learjet was verified by comparing selected data from the ground pulse test to calculations made with the aircraft model. The model was then used to calculate internal cable responses that would be induced by nearby and directly attached lightning. Both test data and analysis results are presented in this report.

This report has been prepared by the Engineering Technology Group of the Boeing Aerospace Companh. The Program Manager was D. E. Isbell; the Project Engineer was J. W. Schomer and the Principal Investigator was Dr. D. F. Strawe.

The authors gratefully acknowledge the contributions of many people in other organizations, whose participation made the successful completion of this program possible.

Mr. Paul Cork of Gates Learjet, Wichita, Kansas, provided invaluable assistance throughout the program, supplying configuration details of the test aircraft required in the modeling analysis.

Mr. William Wadsworth of SRI conducted the cw measurements on the Learjet at KSC and Mr. Rob Bly provided needed information on sensors and sensor wiring.

Mr. Robert Mason and other personnel of NASA Ames were particularly helpful during the two on-site surveys of the test aircraft and in providing needed wiring details of the experimenters equipment installations.

Mr. Larry Walko and other personnel in the AFFDL test organization provided and reduced data from the ground tests and details of the test configuration.

The Project Engineer for the Air Force was Dr. John C. Corbin, Jr. (AFFDL/FES).

iii

78 12 11 041

TABLE OF CONTENTS

LIST OF ILLUSTRATIONS

LIST OF ILLUSTRATIONS (Continued)

SECTION I
INTRODUCTION

This report contains the results of an electromagnetic (EM) coupling analysis of a Learjet that was used as a test aircraft for ground pulse tests and flight tests in a natural lightning environment. External skin currents and internal voltage and current responses are calculated for both the ground pulse test environment and for directly attached and nearby lightning. The calculated responses are compared to measured values for the ground pulse test.

1. BACKGROUND

In 1976, the first joint effort between AFFDL and NASA to obtain information on intra-cloud lightning and its effects on aircraft was initiated as part of the Thunderstorm Research International Program (TRIP-76) at Kennedy Space Center. A NASA model 23 Learjet aircraft was instrumented (under contract to Stanford Research Institute) to measure static electric fields and electrical transients.

In 1977, an expanded joint program between AFFDL and NASA was conducted at Kennedy Space Center as part of TRIP-77 during July and August. The NASA owned model 23 Learjet aircraft was instrumented (under contract to SRI) with E and H field antennas, field mills, and skin current sensors, and special cable runs were installed on the interior of the aircraft to record induced voltages and currents from nearby thunderstorms. Unfortunately, thunderstorms were few and far between in Florida in July and August 1977. As a result, only a limited number of useful measurements could be made.

Concurrent with the 1977 flight program, a ground test program was conducted by AFFDL on the aircraft. To simulate a nearby lightning field, a high-voltage Marx generator was discharged near the aircraft and induced transients from the radiated field were measured on skin surfaces and internal circuitry of the aircraft. To simulate a direct lightning strike, direct attachment tests from a high-current generator were conducted.

As part of the expanded 1977 program, the Boeing Aerospace Company was contracted to develop and apply an EM coupling analysis of the aircraft to predict and interpret magnitudes and waveforms of induced voltage and current transients on the skin of the aircraft for arbitrary simulated lightning sources, the penetration fields that produce voltage sources on interior cables and circuits, and the circuit responses to these sources.

2. OBJECTIVES

The overall objective of the effort described in this report was to develop an analytical EM coupling model of the Learjet test aircraft that could be used to accurately predict induced transient levels on interior wiring produced by a natural or simulated lightning environment. Specifically the objectives were to:

a. Conduct a survey of the test aircraft to obtain the configuration data required to model the external coupling features, the penetrations, and the internal wiring where the induced transients were to be measured during test.

b. Develop an analytical model for transfer functions (1) from an external EM source to skin currents using the computer code WIRANT, and (2) for penetration coupling and internal wire responses using TRAFFIC.

c. Calculate responses to natural lightning and compare to test data obtained during flight test.

d. Calculate responses to simulated lightning and compare to test data obtained during ground tests.

SECTION II
TECHNICAL APPROACH

In modeling aircraft in an EM environment, the induced skin current
and charge densities are first calculated (Figure 1). The calculated skin
current and charge and the associated surface fields are used to drive the
surface penetrations (e.g., cables in wings, wheel wells and empennage,
windows, cracks around doors, skin joints, and other apertures) and the
skin itself when EM field diffusion through it is important. The penetrating
fields produce voltage sources in interior cable bundles. Energy is then
conducted in multiwire transmission line modes to interior equipment. The
techniques[1,2,3] used to model electronic systems in a lightning environment
are virtually identical to those developed over the past 10 to 15 years for
nuclear electromagnetic pulse (NEMP) assessment once the external skin
responses are determined. The basic energy flow and model structure are
shown in Figure 2.

In this analysis, wire grid models[4,5] of the aircraft are used to
calculate the induced skin currents for both directly attached and nearby
lightning. In the past, transmission line models[6] have been used to estimate
the skin responses to attached lightning. That approach treats the lightning
discharge paths as well as the aircraft fuselage and wings as a multibranched
transmission line system with an assumed lightning current imposed on the
lightning line sections. The wire grid approach treats attached lightning as
attached wire sections with an assumed lightning current and represents the
aircraft as a wire mesh approximation of itself. The wire grid model is capable
of providing more accurate estimates of the distribution of current and charge
over the aircraft exterior. Figures 3 and 4 show a wire grid model of a Learjet
aircraft in flight (with gear down). The same model can be used on the
ground by assuming an image plane under the gear (WIRANT 6)[5]. Not shown in
the figures are the wire segment radii which are chosen to properly represent
the inductive and capacitive characteristics of the modeled surfaces. The
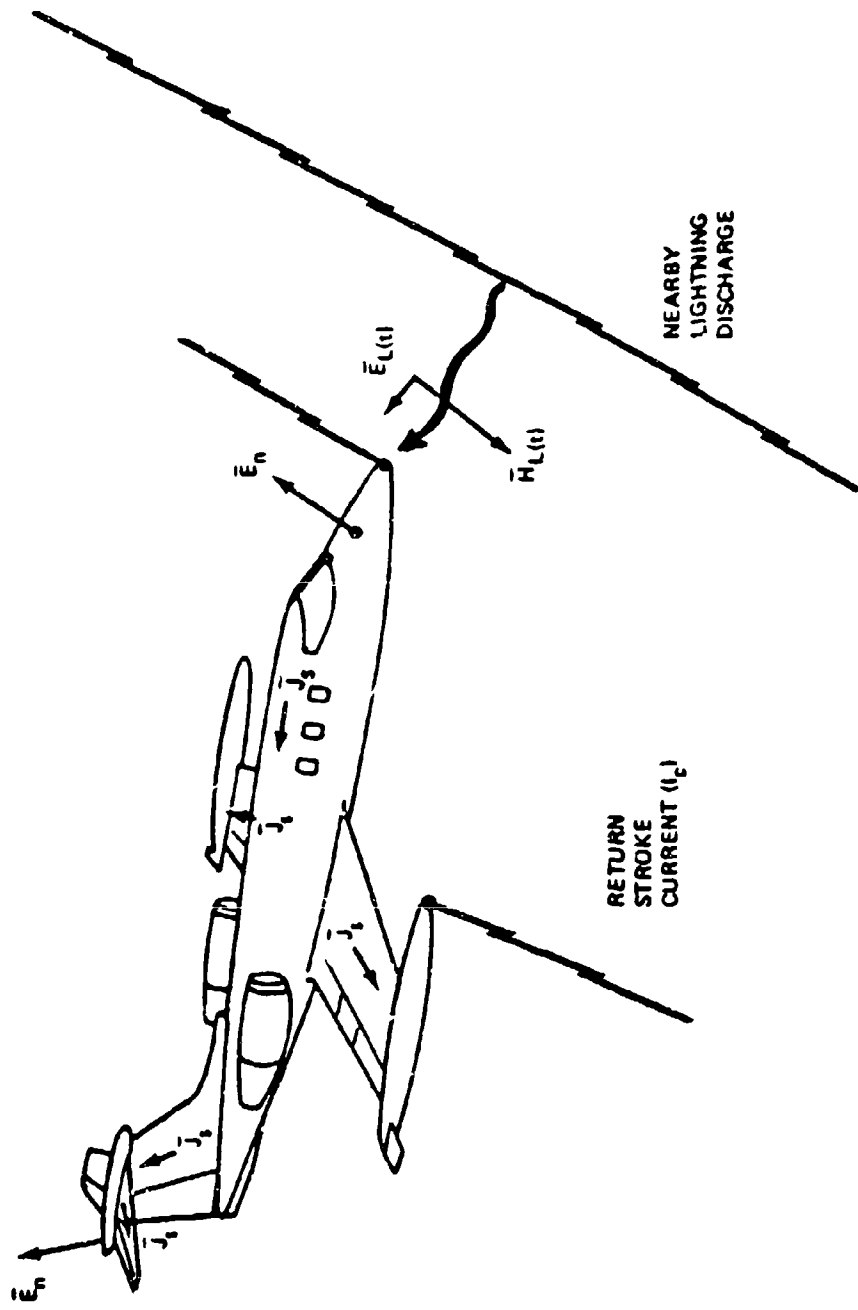skin currents and charge are used to produce voltage drivers in excited

Figure 1. The lightning environment.

4
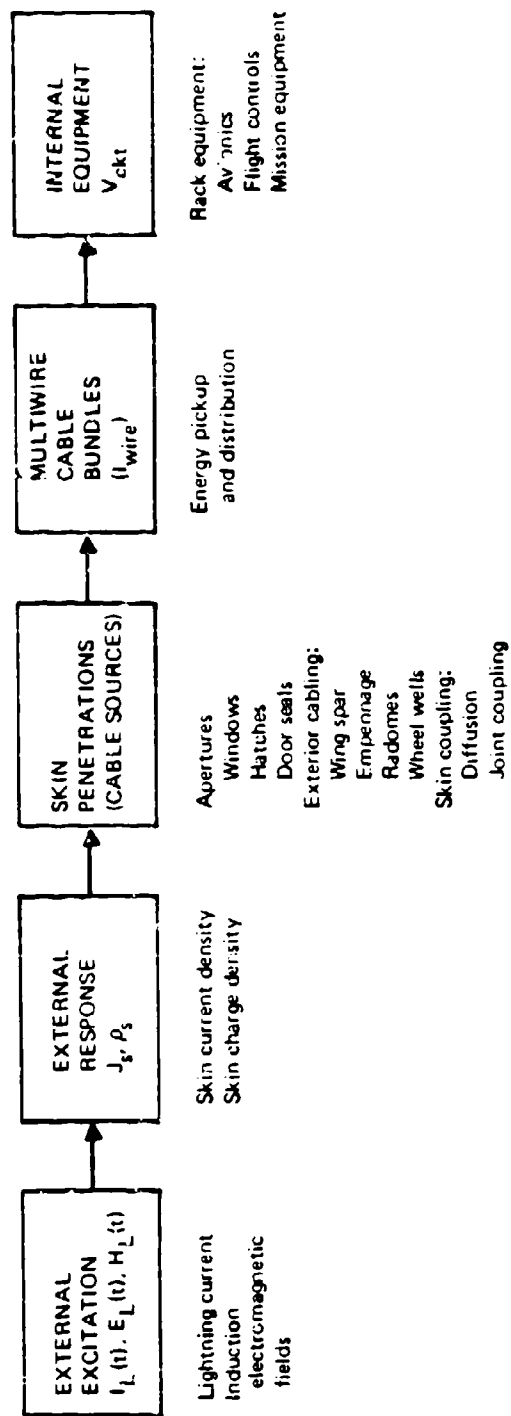
Figure 2. Coupled energy flow path.

5
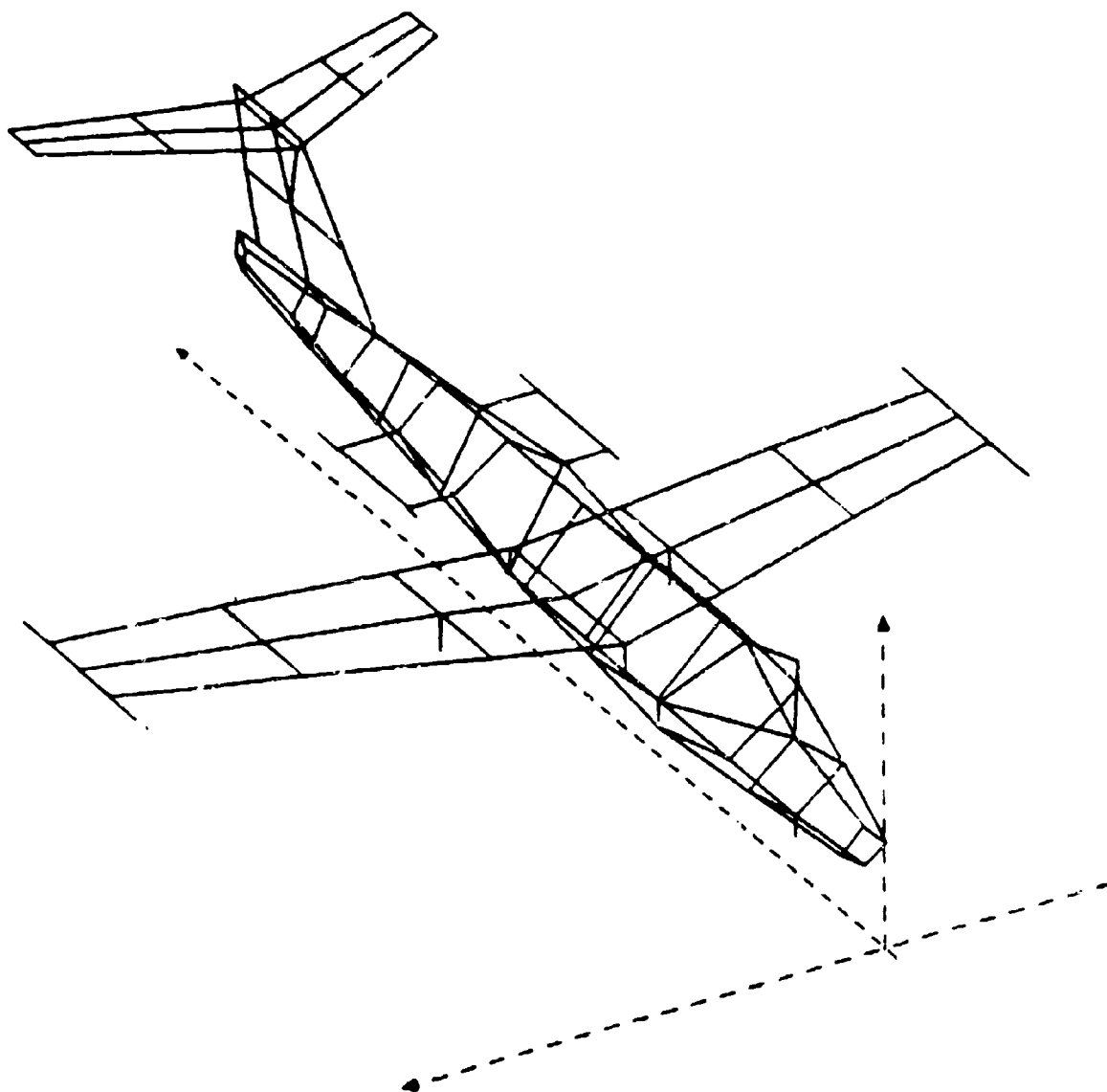
Figure 3. WIKANT model of learjet.
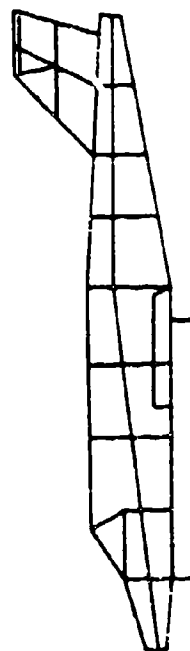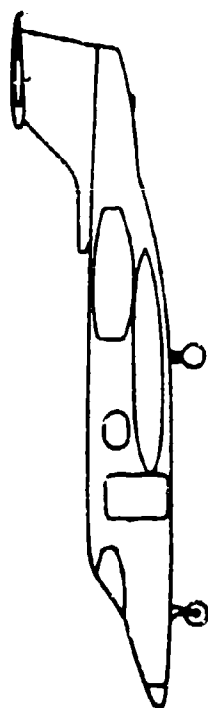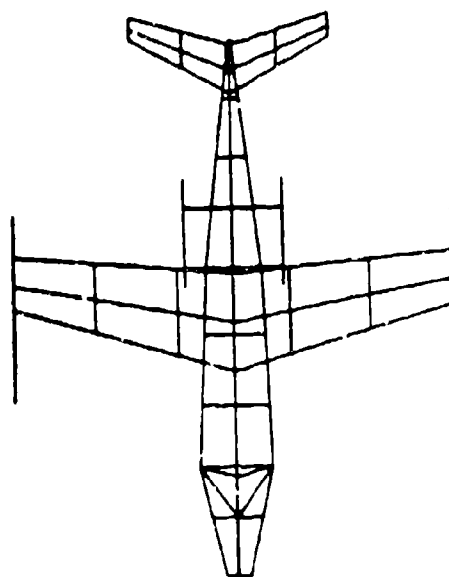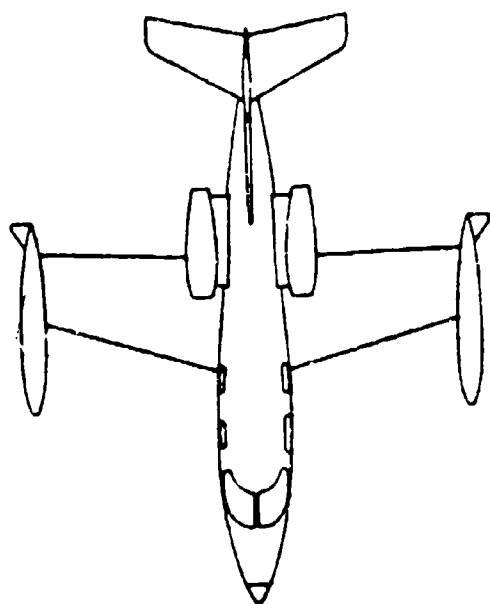
Figure 4. WIRANT model of learjet (continued).

transmission line models[7] of wing (and other) cabling. Skin currents are used with aperture models of windows and skin joints to drive interior cabling. Both electric and magnetic coupling are included in these penetration models. Representative models for the various penetration mechanisms are shown in Figures 5, 6, and 7. Detailed discussions and derivations of these models are available in the literature.[1-8]

Detailed multiwire transmission line models (e.g., from the TRAFFIC network code[9,10]) are used to represent cable bundles. These models are combined with the penetration sources to form Norton equivalent sources at the interfaces between cabling and electrical and electronic equipment as indicated in Figure 8.

Circuit models, damage and upset thresholds, and vulnerability analysis procedures[11] are the same as developed for NEMP. These may be linear "impedance" models when thresholds have been determined at a linear interface somewhat removed from nonlinear circuits or they may be nonlinear (e.g., charge control or Ebers Moll models[12,13] for semiconductor devices) if the interface is very near or tightly coupled to a nonlinear device. The cable models and circuit models are merged and solved to determine circuit responses. Normally, the modeling work is done in the frequency domain. Transfer functions from the exciting EM fields or attached lightning current to circuit responses are calculated and multiplied by Fourier transforms of the excitation. The result is Fourier inverted to obtain the time domain circuit responses. The solution can be accomplished in the time domain with a nonlinear time domain network code such as CIRCUS[12] if the circuit models are nonlinear.

The Learjet was modeled for both flight test and the associated ground test. The internal cabling model is applicable to both. Responses were calculated on wires running to the right wing, to the tail, and to the rear belly area. The interior power cabling system is included in the model

FUSELAGE

SPAR CABLE BUNDLES

CKT

AILERON

FLAP

WING

SPAR

CABLE BUNDLE

FLAP OR AILERON

H_s

E_n

$\odot J_s , \rho_s$

E_n

$[I_s] \sim E_n \sim \rho_s$

$[V_s] \sim H_s \sim J_s$

EXCITATION OF MULTIWIRE CABLE MODEL
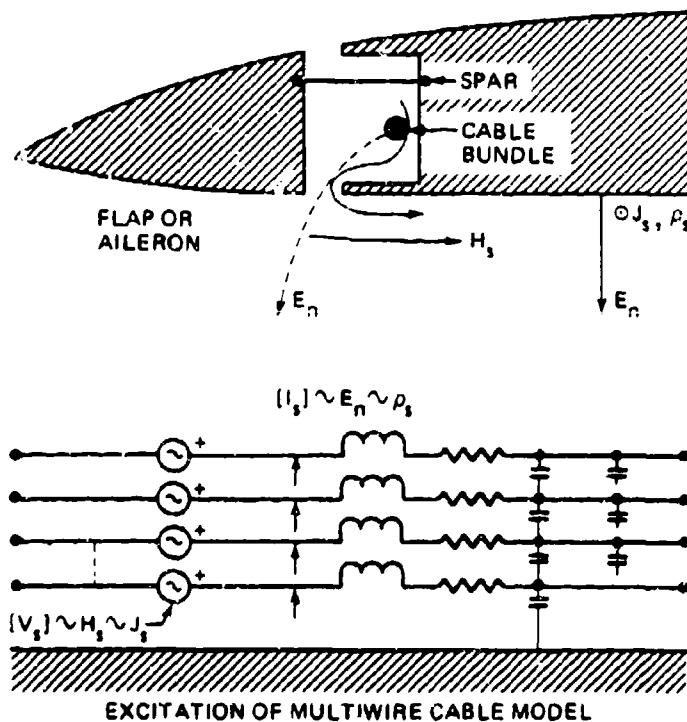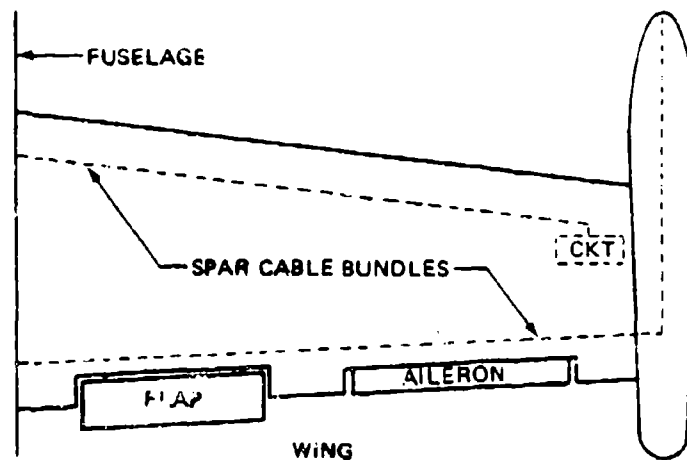
Figure 5. Penetration models—external cable excitation.

9

a) Cable near small aperture

EQUIVALENT DIPOLE
MOMENTS OF
EXCITED APERTURE $\bar{p}, \bar{m}$
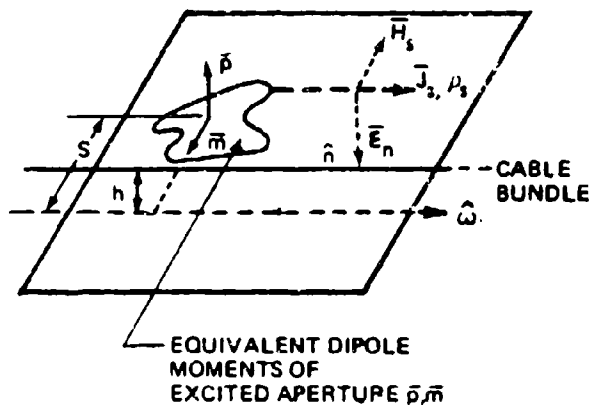
b) Excitation sources

$V_s \sim m \sim J_s \sim H_s$

$I_s \sim P \sim \rho_s \sim E_n$
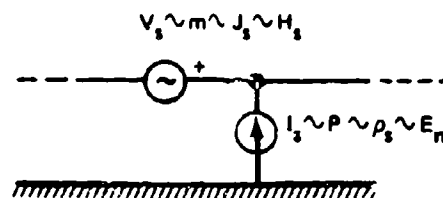
$$V_s = \frac{j \omega \mu h (\bar{\bar{a}}_H \cdot H_s) \cdot \hat{\omega}}{2 \pi (S^2 + h^2)}$$

$$I_s = \frac{j \omega C h a_E E_n}{2 \pi (S^2 + h^2)}$$

$$H_s = \bar{J}_s \times \hat{n}$$

C : CABLE CAPACITANCE/METER

c) Traversed slot, seam, or joint
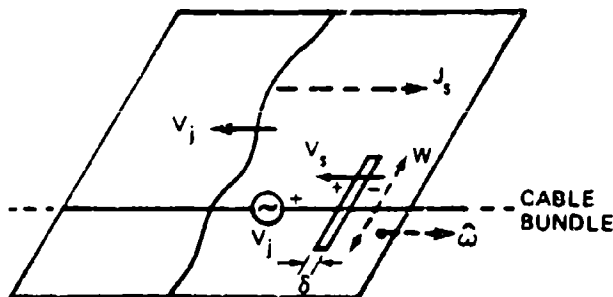
$$V_j = \frac{J_s}{Y_j} \quad , \quad V_s = Z_s \bar{J}_s \cdot \hat{\omega}$$

$$Z_s = \frac{j \omega \mu W^2 \pi}{16 (\ln \frac{4W}{\delta} - 1)} \qquad \text{(THIN SLOT)}$$

d) Elliptical apertures
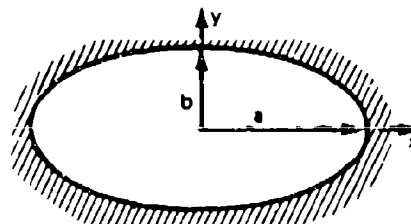
$$a_E = \frac{2 \pi a^3 (1 - e^2)}{3 \, E(e)}$$

$$a_{Hx} = \frac{2 \pi a^3 e^2}{3 [K(e) - E(e)]}$$

$$a_{Hy} = \frac{2 \pi a^3 e^2 (1 - e^2)}{3 [E(e) - (1 - e^2) K(e)]}$$

$$e^2 = 1 - b^2 / a^2$$

Figure 6. Penetration models - internal cable excitation.

10
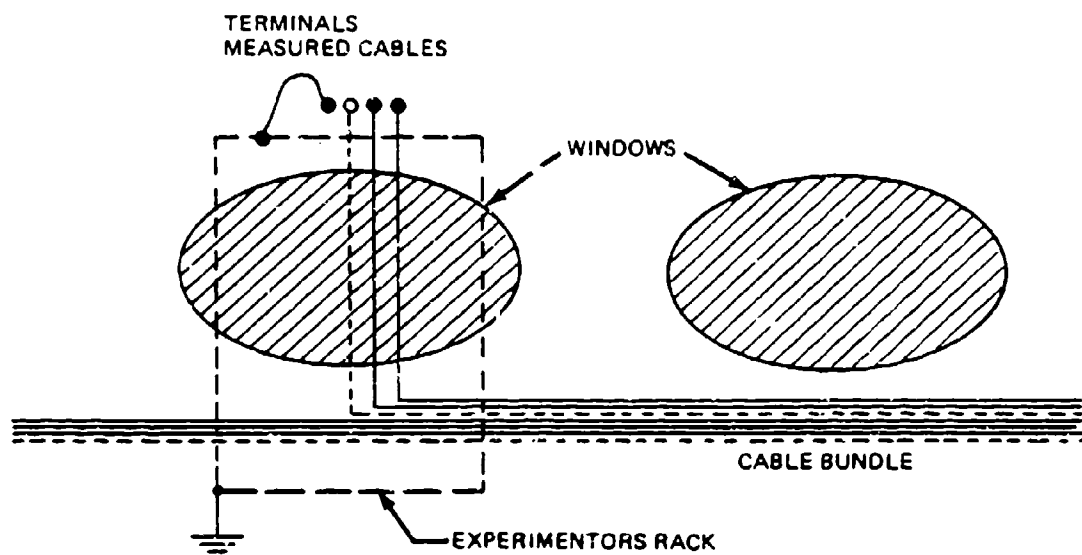
a) Cabin windows-interior view
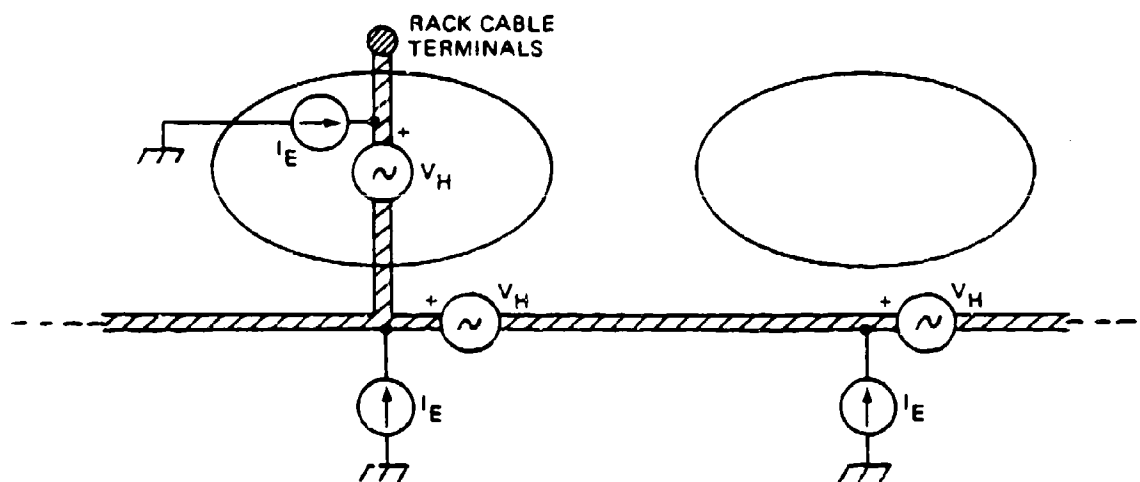
b) Schematic cable representation with sources

Figure 7. Cabin window penetration model.

11
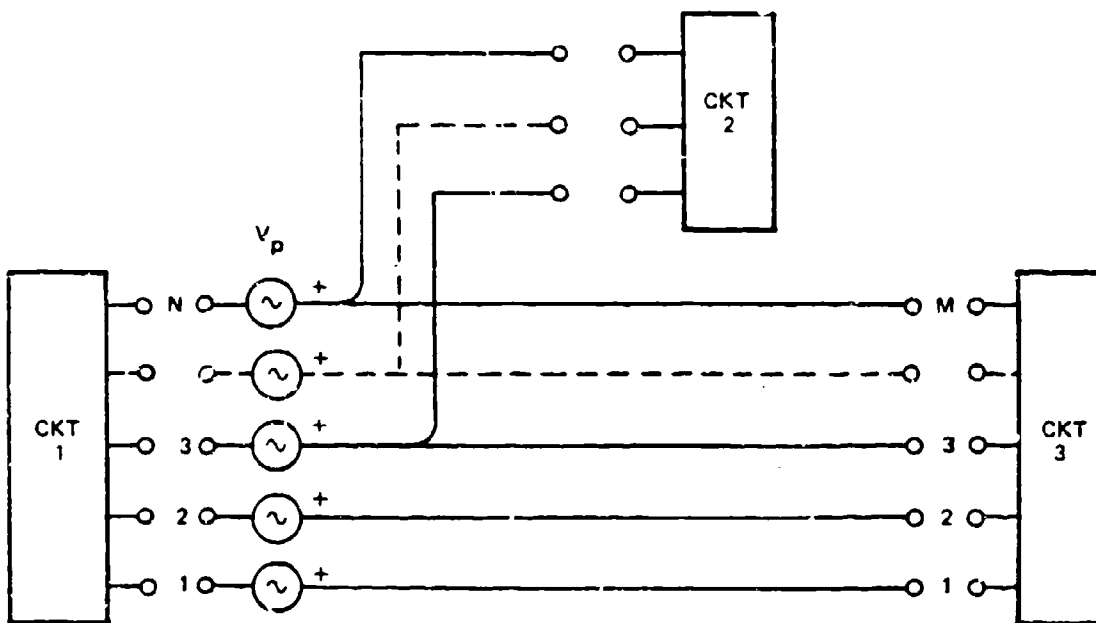
a) Typical model schematic (simplified)

$$[V_C] = \begin{bmatrix} (V_{C1}) \\ (V_{C2}) \\ (V_{C3}) \end{bmatrix}$$

$$[I_N] = \begin{bmatrix} (I_{N1}) \\ (I_{N2}) \\ (I_{N3}) \end{bmatrix}$$

$$[I_C] = \begin{bmatrix} (I_{C1}) \\ (I_{C2}) \\ (I_{C3}) \end{bmatrix}$$

$$[I_C] = [I_N] + [Y] [V_C]$$
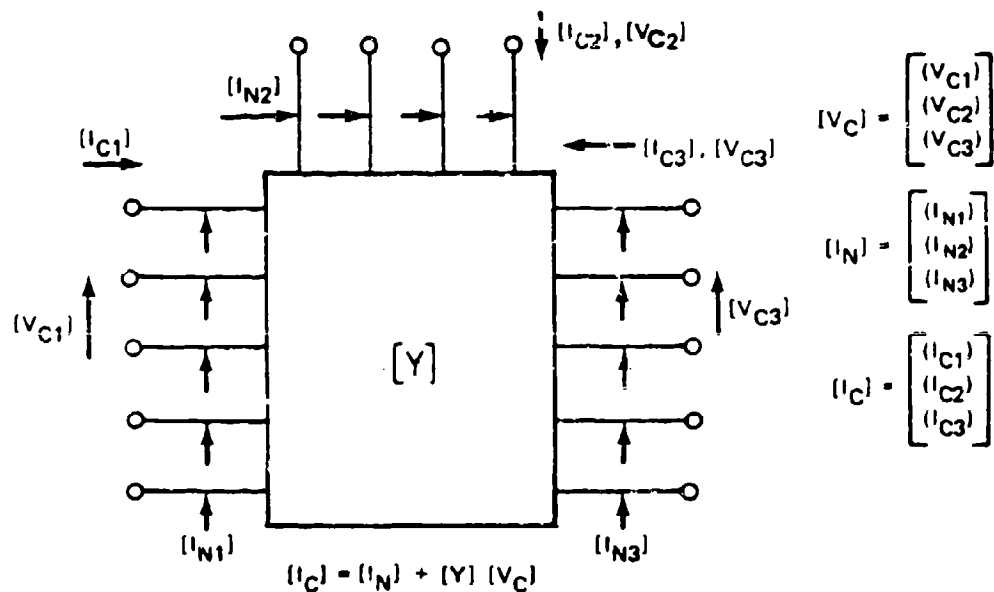
b) Norton equivalent: V-I relations

Figure 8. Multiwire cable models and Norton equivalents.

because the modeled wires were routed along and tightly coupled to it.
Exterior lines running from the interior power system to an external
motor-generator turn out to be the major penetration in the ground test
configuration.

The ground test configuration is shown in Figure 9 along with a
WIRANT model of the aircraft, motor-generator, and the drive array.
The aircraft is driven at its nose against a balanced array of wires
about five feet above ground running around the wing tips and connected
to the aft fuselage end. The WIRANT model of the aircraft is simplified
over the "in-flight" model of Figure 3 to free a sufficient number of
wire segments to model the drive array and motor-generator. The entire
model is taken over an image plane to simulate the effect of the ground.
Ground losses were added as series resistors to the appropriate model
wire segments. Ground resistance calculations follow standard techniques[10,14,15].
Limited ground parametric data were obtained from Patrick AFB; ground losses
became very important since no rebar was used in the hangar floor and pad area
where the ground test was conducted.

The measured input current pulse and its analytical fit are shown in
Figure 10. This current is imposed on the WIRANT model by inserting a high
impedance source in the appropriate array wire segment. Measured and calcu-
lated currents are discussed and compared in Section III.5. The interior
cabling model is driven by coupling to exterior current and charge via the
wing cabling, the tail cabling, and by coupling to cabling in the cabin
through the windows. The primary cable drive in the ground configuration
is cross coupling to the power cabling which is directly connected to the
external motor-generator. The cable model is described in detail in
Section III.3. Measured and calculated wire responses will be presented and
discussed in Section III.5.

POWER
CART
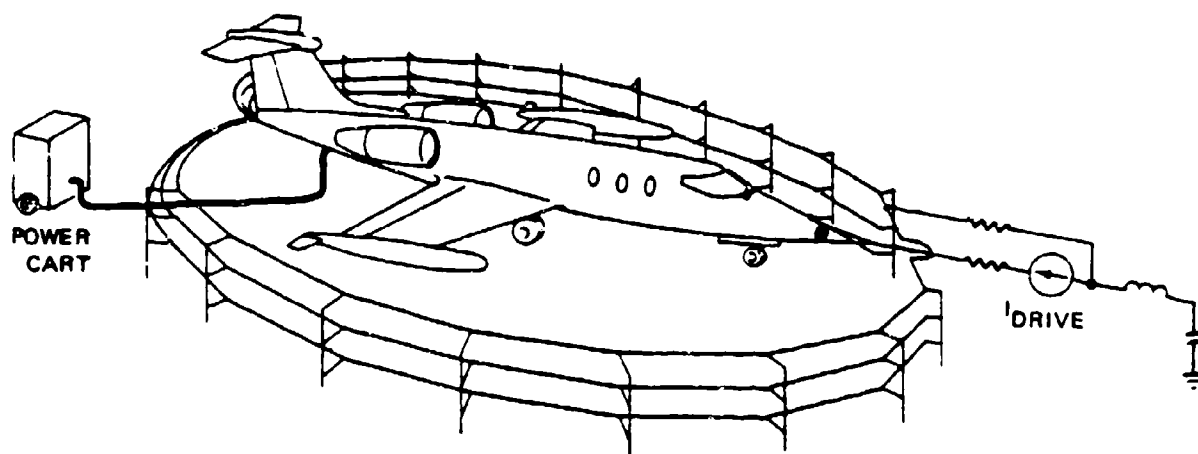
I_{DRIVE}

a)
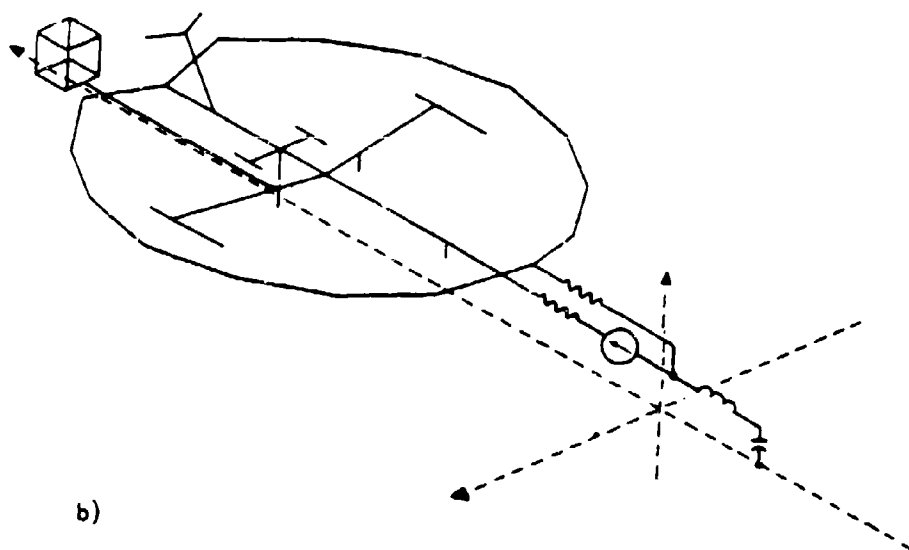
b)

Figure 9. The ground test configuration.

14
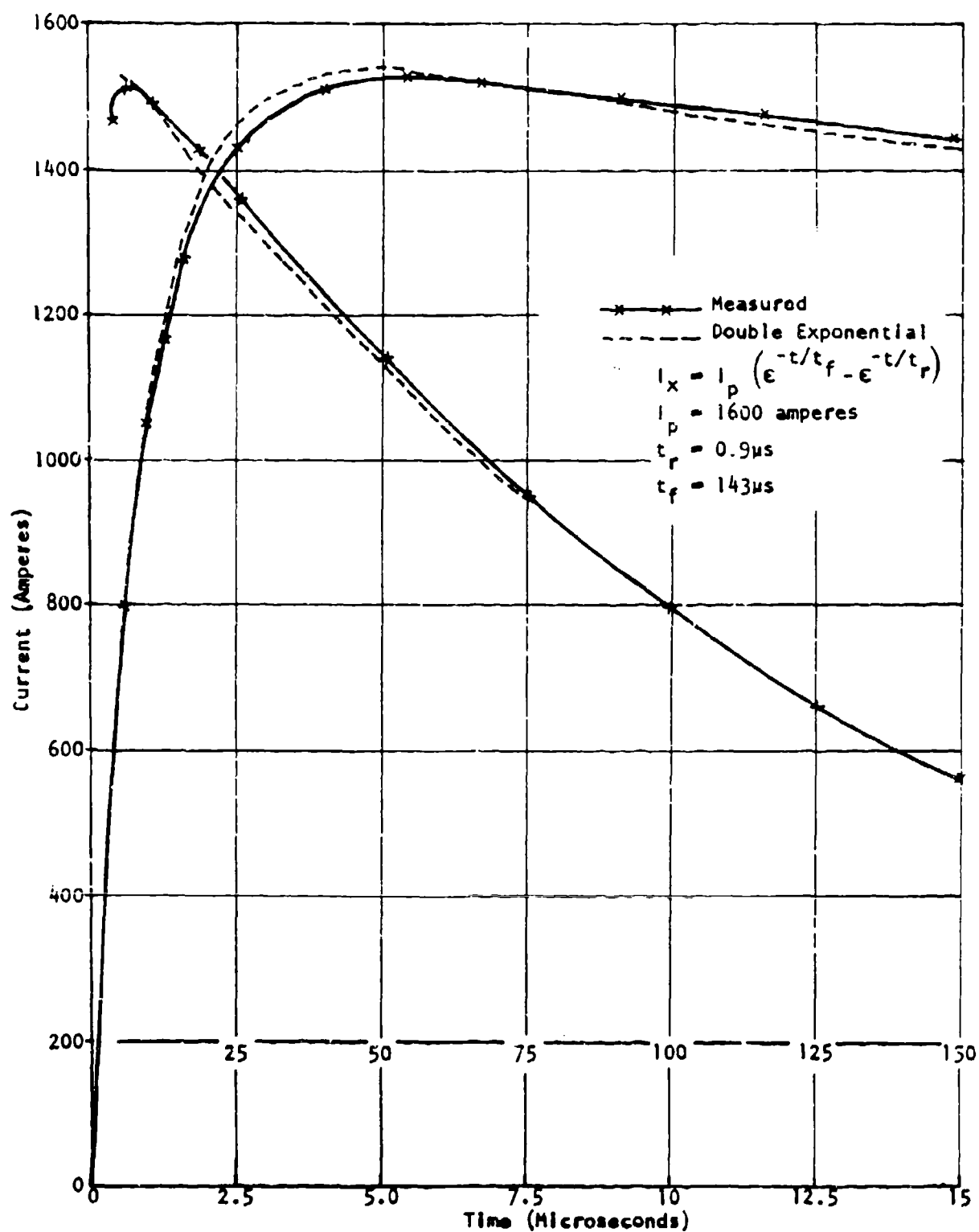
Figure 10. Direct-drive input current.

The in-flight model consists of:

1) The detailed WIRANT model of Figure 3
2) The penetration models of Figures 5, 6, 7, and
3) The cable model discussed in Section III.3
    without the external motor-generator cable and its associated
    excitation.

For directly attached lightning, discharge simulating wires are
attached at selected attachment points and an assumed lightning current is
imposed upon one of them. The form of the model current is a double
exponential. An average initial cloud-to-ground stroke would have, according
to this model,[16] a peak current of about 20 kiloamperes (kA) with a time
to peak of about 1.5 microseconds and a time to half maximum of about 40
microseconds. One percentile extremes would reach 200 kA peak. This lightning
model, with an average 20 kA peak, was used to drive the in-flight model by
direct attachment (nose-wing tip) and indirectly by induction at 100 meters
distance. Calculated right wing and tail wire responses are shown in
Section III.6 (Figures 38 through 40).

Measured in-flight data were examined for comparison, but did not
exhibit the natural resonance responses expected due to the very low signal
levels recorded. All records examined appeared to consist of instrumentation
noise. Amplification only enhanced the relatively slow instrumentation
noise. As a result, the technical effort was limited to modeling the ground
test configuration and calculating certain internal aircraft wire responses.

16

SECTION III
COUPLING ANALYSIS AND RESULTS

1.   EXTERNAL MODELS

External models were required to calculate the external "skin" current
and charge densities on the airplane. Two distinct models were developed -
for the ground test and for the in-flight configurations. The models were
constructed from individual wire segments which formed wire grids or long
cylinders. Excitations were specified for each segment appropriate to the
particular environment for which the airplane response was desired. Currents
on the segments were then calculated using the WIRANT computer code, which is
described in Section II.

In-Flight Model

The in-flight model is shown in Figures 3 and 4. The wings and tail
are modeled as gridded surfaces; the fuselage is represented by a prism-like
approximation to a cylinder. The horizontal tail section is attached as
shown so as to model the hinge/jackscrew attachment details (pitch trim is
maintained in flight by moving the complete horizontal stabilizer through
$\sim 7°$).

Not shown in the figure are the wire segment radii which are chosen
for mesh segments to represent the capacitive or inductive character of the
modeled surface. Engines, tip tanks and landing gear segments use actual
average radii. Segment lengths and grid size were chosen to provide surface
current descriptions for any electromagnetic environment having frequency
components in the 0-20 MHz range.

Environments

1. Direct Strike

Attached lightning or a direct stroke environment was simulated by adding additional segments at the forward end of the right wing tip tank and the nose, representing the lightning column terminations. This attachment configuration was chosen so as to ensure that maximum current would flow on the right wing (exposed test wires on rear spar) and on the forward fuselage (large window apertures). The geometry, loading and sources for the additional segments were chosen so as to impose a Pierce Criterion[16] cloud-to-ground return stroke current of 20 kA peak, 50th percentile. That is

$$I_L(t) = A \left(\epsilon^{-\alpha t} - \epsilon^{-\beta t} \right)$$

where

$$A = 20.6 \times 10^3 \text{ Amps}$$

$$\alpha = 1.7 \times 10^4 \text{ secs}^{-1}$$

$$\beta = 3.7 \times 10^6 \text{ secs}^{-1}$$

2. Nearby Strike

The nearby strike environment was represented by the electromagnetic fields in close vicinity of a cloud-to-ground lightning column.[17] The azimuthal $\vec{H}$ field component, H_ϕ, is described by

$$H_\phi \doteq \frac{I(s) \, \epsilon^{-(\rho+\rho_o)s/c_o}}{2\pi \, (\rho+\rho_o)}$$

The corresponding radial $\vec{E}$ field is

$$E_\rho = I(s) \frac{60}{(\rho+\rho_o)v_f} \left(1 + \frac{1}{st_s} \right) \epsilon^{-(\rho+\rho_o)s/c_o}$$

$I(s)$ describes the current after $t = 0$ at elevation $(z + z_o)$ as follows.

$$I(s) = \frac{I_L(s)}{c_o v_f} \epsilon^{-(z+z_o)(s + 1/t_s)}$$

where $I_L(s)$ is the Laplace transform of $I_L(t)$ described earlier. The airplane was placed at 1000 meter elevation and 100 meters from the column which is likely to be the distance of closest approach without being directly struck. Parameter values were:

c_o free space velocity of propagation ($\sim 3 \times 10^8$ m/s)

$(\rho_o + \rho)$ distance from column to centers of wire model segments ($\rho_o = 100$ m)

$(z+z_o)$ distance from ground to centers of wire model segments ($z_o = 1000$ m)

v_f velocity factor on lightning column (.3)

t_s attenuation height index on column (.5 $\times 10^{-4}$)

The airplane was oriented in a "fly by" position i.e., the left wing axis was pointed at the lightning column.

Ground Test Model

The ground test model is shown in Figure 9. The airplane was driven at its nose against a balanced array of wires about 5 feet above ground running around the wings tips and connected together to the aft end of the fuselage. The pulser was connected to the nose and return wires through a 20 ft drive line. Power for onboard instrumentation during the test was provided by a motor generator set connected through a power cable $\sim$ 23 feet in length to the airplane external power receptacle. All of these features were of significance in determining how the pulser current distributes on the aircraft and were included in the model.

The model of the aircraft itself, when compared to the in-flight model, is greatly simplified - all meshing has been eliminated leaving a one dimensional stick representation. This was required so that a sufficient number of segments were available to model the additional features. The entire model was placed over an image plane ($\sigma = \infty$) to simulate the effect of the ground. Segment lengths were chosen so as to be electrically short ($< \lambda/6$) up to 20 MHz.

The simple cylinder representation for the wings inadequately modeled the ground capacitance; wing segments parallel to the fuselage are therefore included. Similarly, vertical segments were added to the cylinder representing the screen wires - in this case the wing to screen capacitance was improved. The screen array was in reality four small wires spaced approximately 12 inches apart overall. The inductive behavior was well represented by a 12 inch diameter cylinder.

The pulser, which was composed of 12 high voltage capacitors in parallel, was modeled by an equivalent .5 uH lead inductance and 200 pF capacitance to ground. The measured input current and its analytic fit are shown in Figure 10. This current was measured on the drive line side connected to the airplane nose. It was imposed on the wire model by inserting a high impedance voltage source in the appropriate segment.

The power cart shown in Figure 9 was modeled as an open box 4 ft high whose base is 6 inches above the ground plane. The cable connecting to the airplane was a thickly insulated, 2 conductor type. It lay, for most of its run, directly on the concrete. In line with past experience with cables of this sort a characteristic impedance (Z_o) of 100Ω and velocity factor of .5 were judged appropriate. Segment radius, height and additional capacitance to ground were then calculated. Adding additional capacitance to ground was done by inserting segments connecting to the ground plane at three places along the cable. These added segments were then capacitively loaded.

Losses

The entire model was placed over a perfectly conducting ground plane. In reality, the ground inside the Patrick AFB hangar had no rebar in the concrete and was composed of three identifiable layers - 8 inches of unreinforced concrete, 10 ft of semidry sand below which was the water table (sea water). Transmission line calculations with this configuration of ground return and conductivity gave circuit Q's of 4 to 5.

No such loss mechanism in the ground plane can be directly included in a WIRANT solution. Instead, equivalent loss calculations were made in an approximate way for the segments in the model. Those losses were then included by inserting resistors in many of the segments.

Specifically, this calculation was made for each large piece of the model (e.g., the airplane fuselage) by calculating a Z_o, then solving for the loss required per unit length with the given Q using the approximations of low loss transmission line theory. The wire return array skin losses were included by adjusting the conductivity of the single cylinder representation, on an equivalent loss basis, i.e.,

$$\sigma_2 = \sigma_1 \, [4 \; D1/D2]^2$$

where σ_2 adjusted conductivity for single big cylinder
σ_1 conductivity for copper wire (4.8×10^7 mhos/M)

D_1 diameter of return array wires (#12)
D_2 diameter of model cylinder

Ḣ Field Calculations

External "skin" current density measurements were made with Ḣ sensors located on the forward and aft fuselage, and on the wings. The modified stick model of the airplane yielded a current which required division

21

by an appropriate perimeter factor to give an H field. $\dot{H}$ was subsequently found by multiplying by $j\omega$ before the inverse transforms were taken.

The fuselage perimeter factors were related in a straightforward way to the local fuselage diameter, i.e., $P_f = \pi D$ where D is the fuselage diameter at the locations of the forward and aft sensors. For the wing sensors, the wire segment current was nonuniformly distributed over a thin elliptical approximation to the wing cross-section near the wing root. At distance x from the center (measured along major axis)

$$H(x) = \frac{I}{2\pi \sqrt{a^2 - x^2 e^2}}$$

where
$\quad I$ = segment current

$\quad a$ = semi-major axis

$\quad e$ = eccentricity $\sqrt{1 - b^2/a^2}$

$\quad b^2$ = semi-minor axis

2. PENETRATION MODELS

As indicated in Section II there are numerous "penetration" or entry points through which exterior aircraft EM surface fields can enter the aircraft interior. Analysis shows that, for the particular interior responses selected for modeling, the major pen .rations are wing spar cables, the cabin windows, and the external power cables (ground test only). In order to facilitate measurement and simplify model data requirements, wires were "layed in" along existing aircraft cabling to field mill locations at wing tank tips, tail, and forward and aft belly locations on the fuselage. Excluding the ground power cables the only significant sources for these cables are the cabin windows and right wing spar fields.

The penetration model for the cabin window (Figure 7) consists of voltage sources in series with each modeled wire running nder or across the windows. This is a Faraday voltage following the time derivative of the

22

magnetic field leaking into the cabin. Also, electric field leakage through
the windows is represented by shunt current sources injecting (displacement)
current into each modeled wire. The cable source model is detailed in
Section III.3 (Figure 13). The wires running under and across the windows
have sources determined by the model described in Figures 6 and 7. Specific
aperture susceptibility factors for 6b) were obtained from the expressions
of 6d).

The form of the right wing excitation model is indicated in Figure 5.
The cable bundle is dressed along, and about 1 inch above the rear spar.
The spar itself is recessed from the wing edge by approximately 3 inches.
This recessed geometry and the adjoining flap (or aileron) structure provides
a substantially larger degree of shielding (Farada of the local electric
field than of the local magnetic field. For this reason, electric coupling
to the spar cabling has been neglected. This approximation has been
successfully used in most previous aircraft modeling programs at Boeing. As
indicated in the figure, the wing cable penetration model consists of series
distributed voltage sources in each modeled wire. At a given location, all
wire sources are identical functions of position along the cable run and
proportional to the local magnetic field on the wing H_s. The induced
voltage per unit cable length is calculated from Faraday's law.

$$\frac{\partial V_s}{\partial x} = j\omega\mu h f\, H_s$$

where h is the wire (bundle) to spar spacing and f is the shielding ratio
of the spar and wing exterior. The ratio (f) of exterior wing H field to
spar H field threading the cable-spar loop was estimated here as about
1/3 or -10 dB in the flap up configuration. The cable model is composed
of electrically short tandem transmission line sections of length L. A
single lumped voltage source V_s is entered into each section.

$$V_s = \frac{\partial V_s}{\partial x} L$$

In the ground test, an external power cart is used to provide power to the on-board instrumentation. Cables from the cart penetrate the aircraft near the hell hole door on the aft belly. In addition to supplying dc power, they conduct large amounts of induced current (approximately 30 amperes per cable) into this aircraft cabling system. The "penetration model" in this case is merely a direct connection through the aircraft power connector of the Norton equivalent of the external cable at the connector to the internal power system model within.

3.   INTERNAL CABLE MODELS

The aircraft and cable configuration data required to construct a coupling model for the Lear was obtained from drawings supplied by Gates Learjet, Wichita, Kansas, at the beginning of the program, and from an on-site survey of the aircraft before the tests at Kennedy Space Center. Initially data was obtained only to model the special test cabling layed-in for the field-mills and skin current sensors. Later when it was evident from inspection of the ground test data that the cable to the power cart was coupling large amounts of energy into the aircraft wiring, it was necessary to survey the aircraft again after the tests were completed and to visit the Gates Learjet plant to obtain needed details on the power system wiring.

In preparing the aircraft for testing, test wire bundles were run from the instrumentation rack located just opposite the door on the right side of the cabin to field mill and skin current sensors placed on the aircraft. The test bundles routed from the rack to both right and left wings, forward and aft belly, and to the tail. Where possible, they were layed in along side the standard Lear wiring taking advantage of existing cable routing. Figure 1: shows the cable routing in the aircraft.
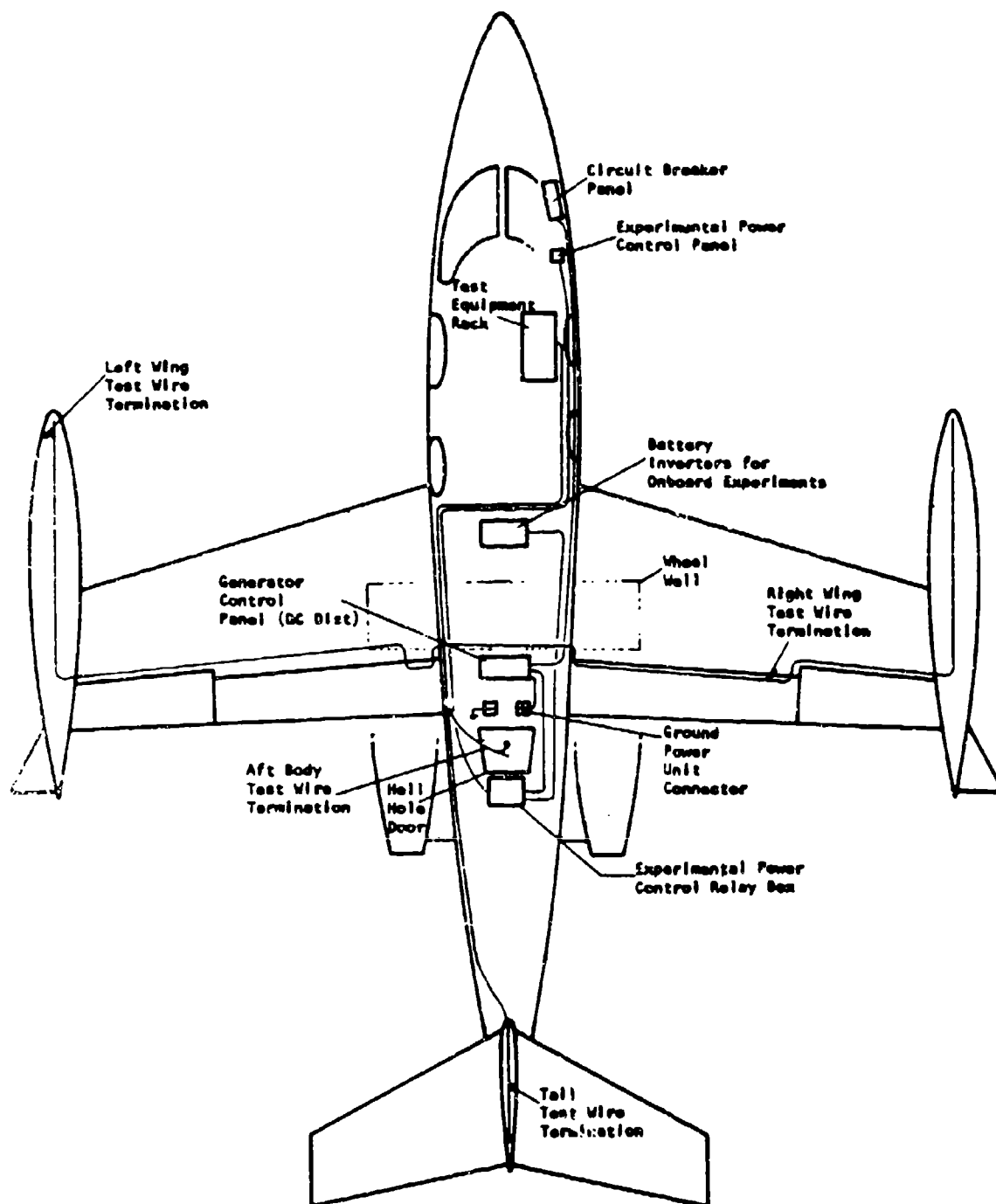
Figure 11. Learjet internal wiring.

25

Each field mill required both a control cable consisting of a
bundle of eight conductors in an overall insulating shield and, like the
skin current sensors, a miniature coaxial cable. Two individual #22 con-
ductor test wires were carried along with each bundle and terminated at
the field mills. One was terminated directly to aircraft frame in a short
circuit and the other to aircraft frame in a 68 Ω resistor.

The two individual conductors to the right wing were reconfigured
to run behind the flaps along the trailing spar of the right wing instead of
inside the wing box as in the left wing. They were tied in along with a
Lear bundle running along the rear spar and were terminated centerboard
on the wing in a short circuit and a 68 Ω resistor, like the others. Figure
12(a) shows a photograph of the two right wing test wires running with the
Lear bundle and Figure 12(b) a photograph of the wire terminations.

In the absence of coupling from the power system two major sources
of coupling to internal test cabling were recognized. The cable bundles
running in the cabin were exposed to coupling from electric and magnetic
fields from the windows acting as apertures. The individual test wires
reconfigured to run along the rear spar of the right wing received magnetic
field coupling due to currents flowing on the wing.

The complicating feature of the aircraft dc power system resulted
from the configuration of the onboard test equipment power system. This
power system allowed for power to the test equipment to be drawn from the
main aircraft dc bus system or an external power source. The system was
controlled by a relay box mounted just aft of the "hell hole" door (aft
equipment bay door) and a switch control panel on the copilots side of the
cockpit. The two were connected by a seven individual conductor cable bundle
that was tightly tied to the layed-in test bundles for length of the cable
run from the aft equipment bay up to the test equipment rack.
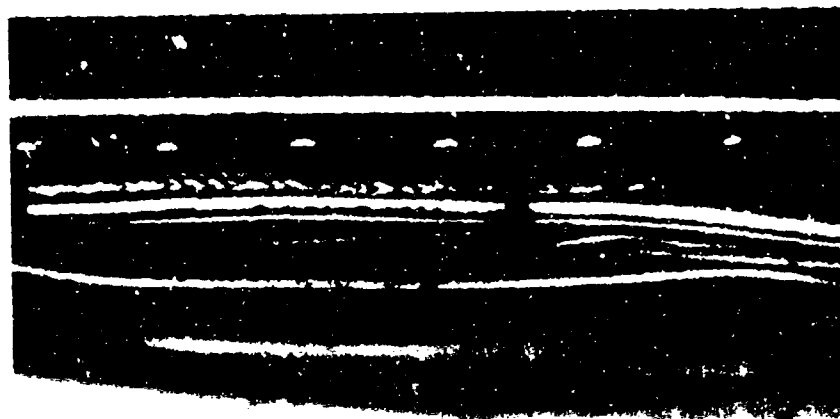
a) Wires along flaps
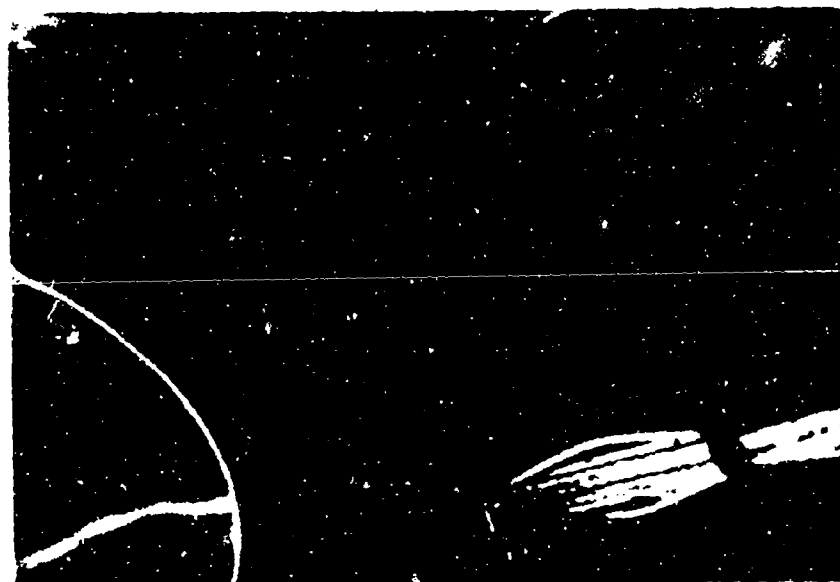
b) Termination on flaps

Figure 12. Right wing test wires.

During the ground test the aircraft dc bus system was powered by the external motor generator with the experiment power system switched to draw power from the dc bus system. Consequently, external excitation at the ground power connector penetration resulted in mutual coupling of power system transients into the test bundles. The close proximity of the aft belly test bundle and termination to power cables in the aft equipment bay also resulted in significant mutual coupling from the power system to that cable.

In order to perform the coupling analysis of the Learjet internal cabling system the PRESTO[10] system of computer codes was employed. PRESTO consists of a unified set of application codes, each performing a specific step in the analysis procedure.

In this analysis, the application code WIRANT was first used to derive the aircraft external currents for both ground test and inflight configurations. The data editor, PRIDE, was then used to modify the calculated external currents by analytical expressions that relate those external currents to induced voltages and currents on the exposed internal cabling. The applications code TRAFFIC was employed to model the internal cabling of the aircraft. The TRAFFIC output contained the voltage and current measurements at the desired test points. They were, however, in the form of frequency domain spectra and had to be transformed into the time domain by DRIFTR, the Fourier transform package. The CAPSULE code was then employed to provide time and frequency domain plots of the output.

In building the computer model of the aircraft internal cabling both TRAFFIC and its adjunct, TML, were employed. TRAFFIC (Transfer Functions for Internal Coupling) was created to perform frequency domain analyses of linear electrical networks. The TRAFFIC Modeling Library (TML) consists of a set of analytical equations that were used to calculate electrical equivalent circuits of multiwire transmission lines (cables) and the coupling of the transmission lines to an electromagnetic field environment. TML provided

28

the transmission line equivalent circuits of the cables for use by TRAFFIC. The equivalent circuits of the loads terminating each cable were input into TRAFFIC as discrete resistor, inductor, and capacitor elements.

The transformation of the physical configuration detailed in Figure 11 into a computer model is shown in the TRAFFIC block diagram, Figure 13. The blocks labeled *MWTL are multiwire transmission line equivalent circuit blocks modeled using TML. The other blocks represent the equivalent circuit loads of the cables. Each transmission line block models a discrete section of cable. The nodes on each block correspond to individual wire conductors or groups of conductors shorted together in the common mode. The nodes on the transmission line blocks and loads are then connected together in a manner that is topologically analogous to the physical configuration. The cable paths from the bottom of Figure 13 to the top correspond to:

    Test equipment bay to left wing
    Test equipment bay to right wing
    Test equipment bay to tail
    Test equipment bay to aft belly
    Experimental power switch panel to experimental power relay box
    Cabin circuit breaker panel to dc bus system

For example, the photograph of the cable section running along the rear spar of the right wing (shown in Figure 12(a)) is modeled by blocks RWBA, RWBB, and RWBC. The nodal pairs 1,13 represent the Lear bundle (common mode) and the two pairs 11,23 and 12,24 represent the individual test wires. The cable is terminated in block RWLOAD.

Previous experience in modeling aircraft internal cabling has shown that a reasonable treatment for cable bundles where information is not known about all of the terminations is to treat them in the common mode and apply 20 Ω as a bulk load for the cable terminations. The Lear bundle along the right wing was treated in this manner as were others in the model.

Figure 13. Learjet cable model-block diagram .

The model is driven by four source blocks for the ground test configuration. Blocks AA and BB model the distributed magnetic coupling of the right wing wires. The WINDOW block provides the electric and magnetic field aperture sources to the cabin cables. Block GPU is a Norton equivalent circuit of the ground power unit penetration to the dc bus system. This block was replaced by a small impedance to frame for the inflight model. For a short description of the function of each block in the model see Appendix A.

The calculated responses were made in block TESTBAY for the right wing, tail, and aft body test wires. The wires that were far-end terminated in a short circuit were measured for short circuit current and the wires far-end terminated in 68Ω were measured for open circuit voltage. The short circuit current and open circuit voltage measurements were performed simultaneously for the right wing and for the tail. Only the short circuit current was measured for the aft body.

4.   MODEL INTEGRATION

The external WIRANT model was used to calculate the airplane skin currents given the external environment and connections (III.1). The internal TRAFFIC model predicted voltages and currents at specified nodes for an arbitrary source in the network (III.3). The currents found in the external model were related to the sources in the internal model by the penetration transfer functions (III.2).

Initially the external and internal models were constructed, checked out and run independently. Port impedance calculations (measured voltage for unit current source) were used to verify the internal model. When both models were working satisfactorily, the external model currents were stored on computer disc files and accessed as required by the internal model. The internal model set-up routines contained the penetration transfer functions which were required to calculate sources. On-going development of both models could then proceed, with a new WIRANT current file saved at appropriate times.

31

5.   GROUND TEST CALCULATIONS

a. Exterior Responses

The structure of the wire array used to drive the aircraft is indicated in Figure 9. The array input current I_{DRIVE} was measured and serves as a source current for the model. Strictly speaking, since the pulser and aircraft are coupled to ground, both a line to line (differential mode) and line to ground (common mode) modes exist on the two drive cables connecting the pulser to the array. In consequence, it is necessary to measure (and specify to the model) both drive cable currents. This was not done; only one current was specified to the model as a source with a resulting high frequency error in the model. In addition, the drive current record used was in the form of "scope photos" with time scales 2.5 and 25 microseconds per division. This gives inadequate resolution of the initial phase of the pulse and in turn the HF ($f > 1$ MHz) part of its spectrum. To exemplify this fact, a second data fit was used for all model calculations. This is a triple exponential with third turning frequency of 2.5 MHz. It starts in a more physically credible manner with zero slope at the starting time but follows the data closely everywhere. The double and triple exponential curves are compared in Figure 14.

The measured array drive current and its double exponential curve fit are shown in Figure 10. Time derivatives of forward and aft belly skin current densities were measured as well as that of the right wing underside. These measured data are shown in the upper plots in Figures 15, 16, and 17. Their calculated counterparts obtained from the "stick model" of Figure 9 are shown in the bottom plots in these figures for double exponential drive. Response to the triple exponential responses appear in Figures 18, 19, and 20. All these exterior aircraft skin current density data were kept in the time derivative format of the measurements (rather than integrating to yield skin current densities) because that format better displays the high frequency components which dominate interior cable responses.
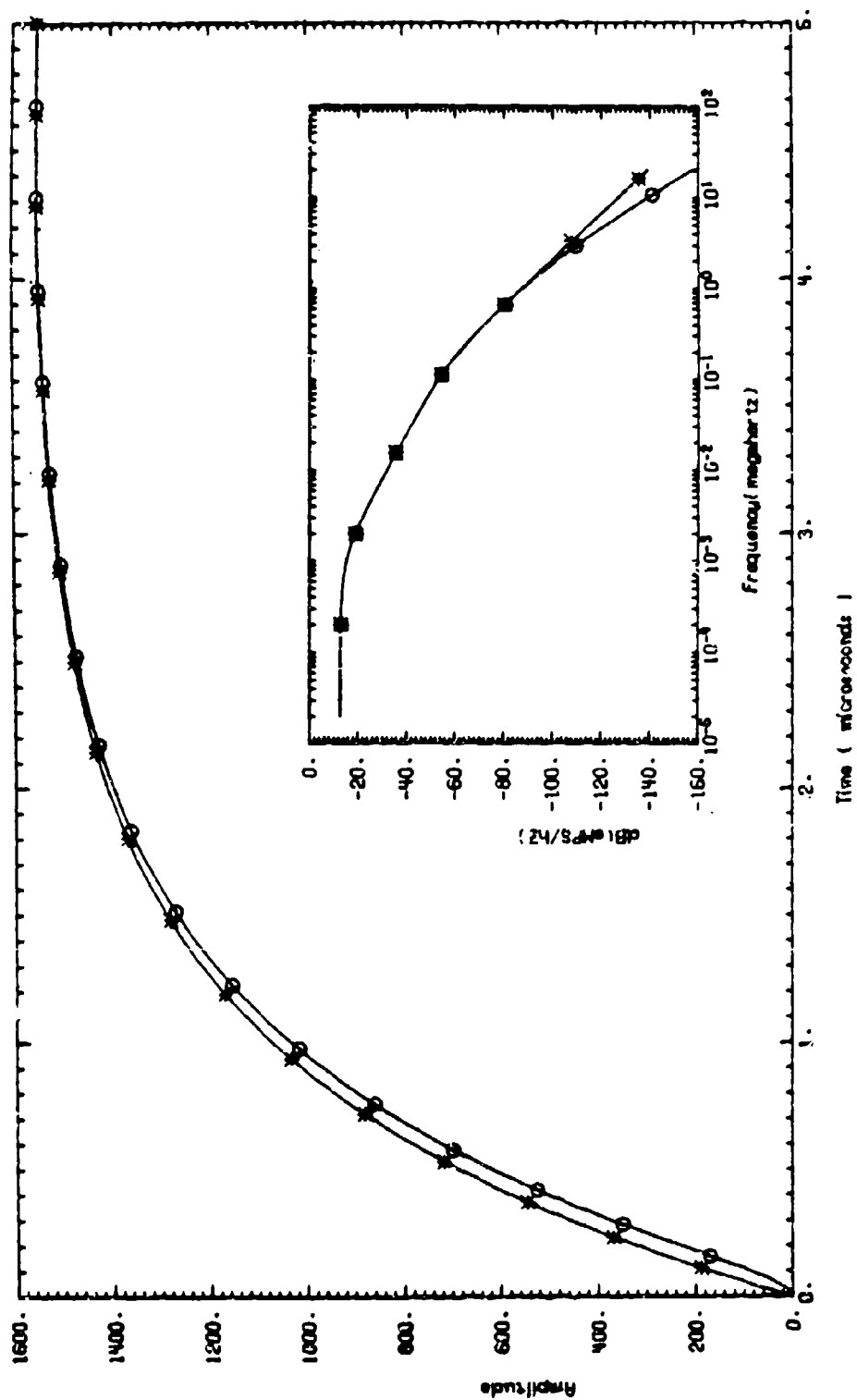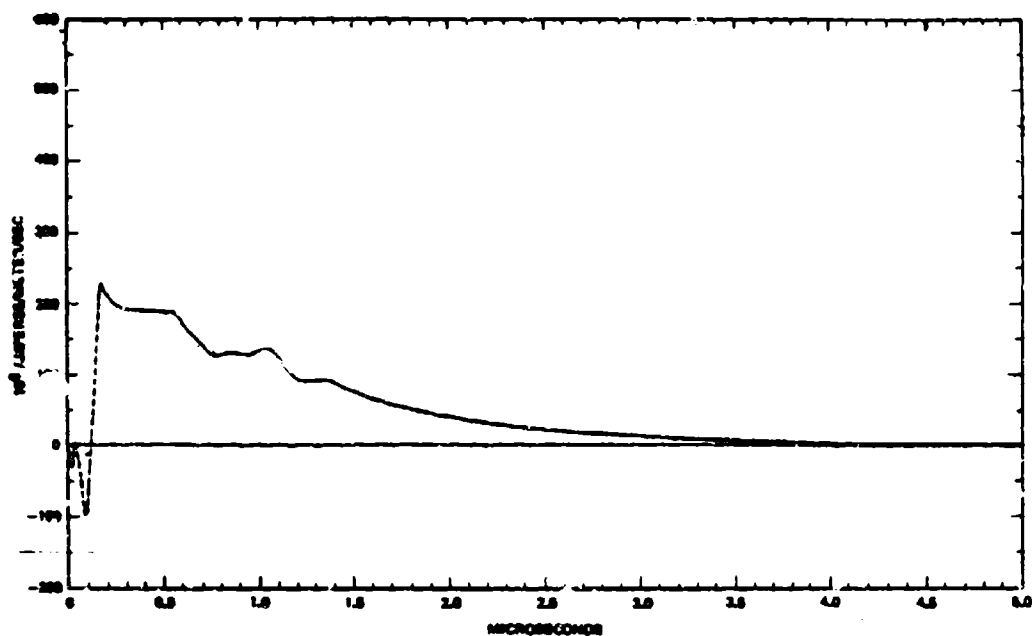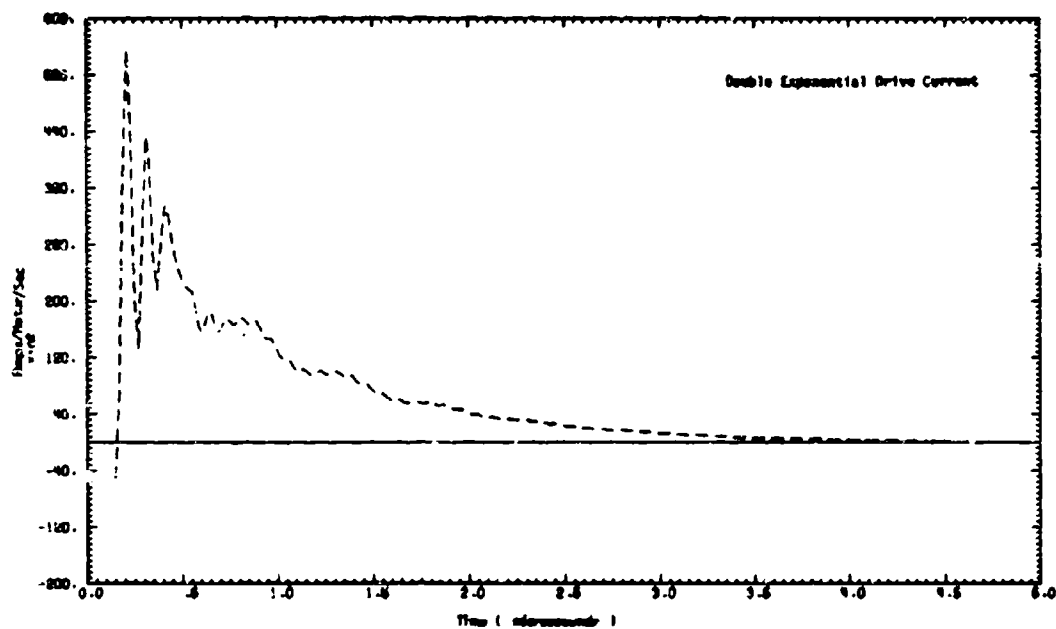
Figure 14. Double and triple experimental representation of input pulse in frequency domain.
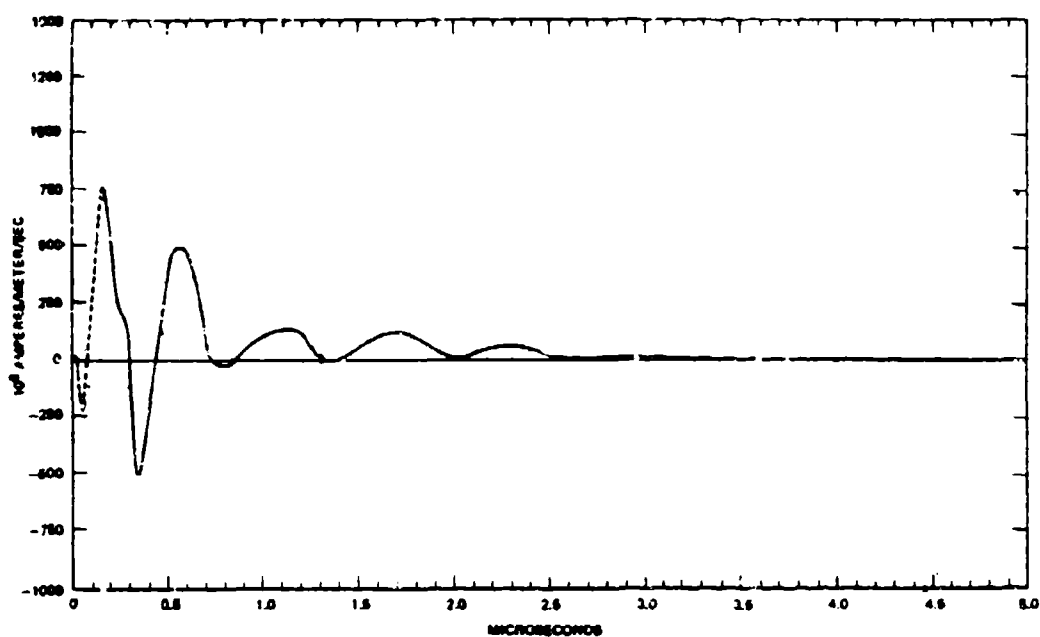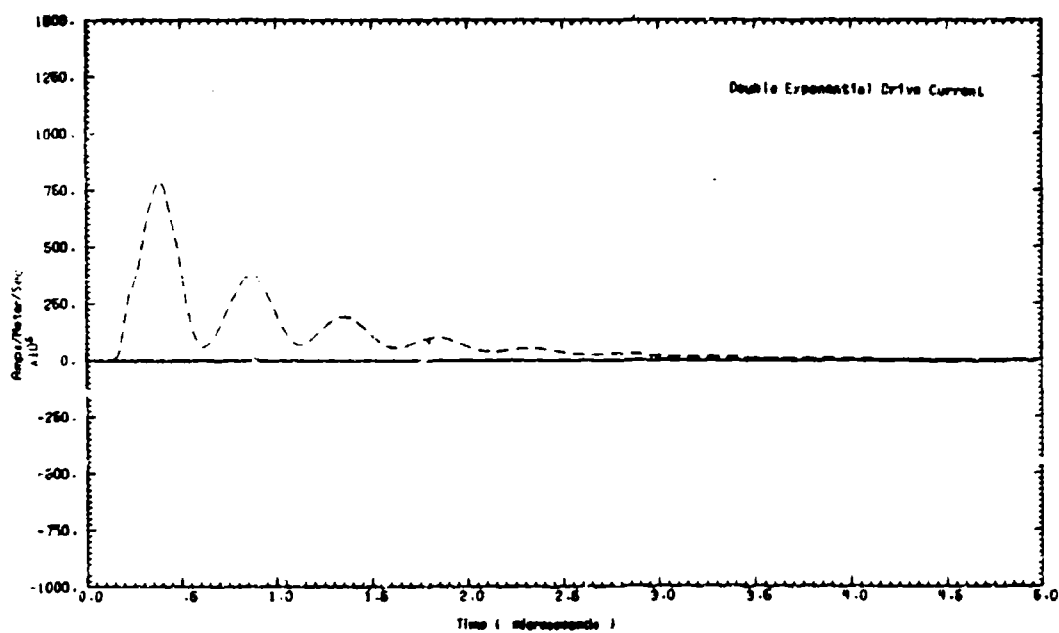
a) Ground test data

b) Calculated response

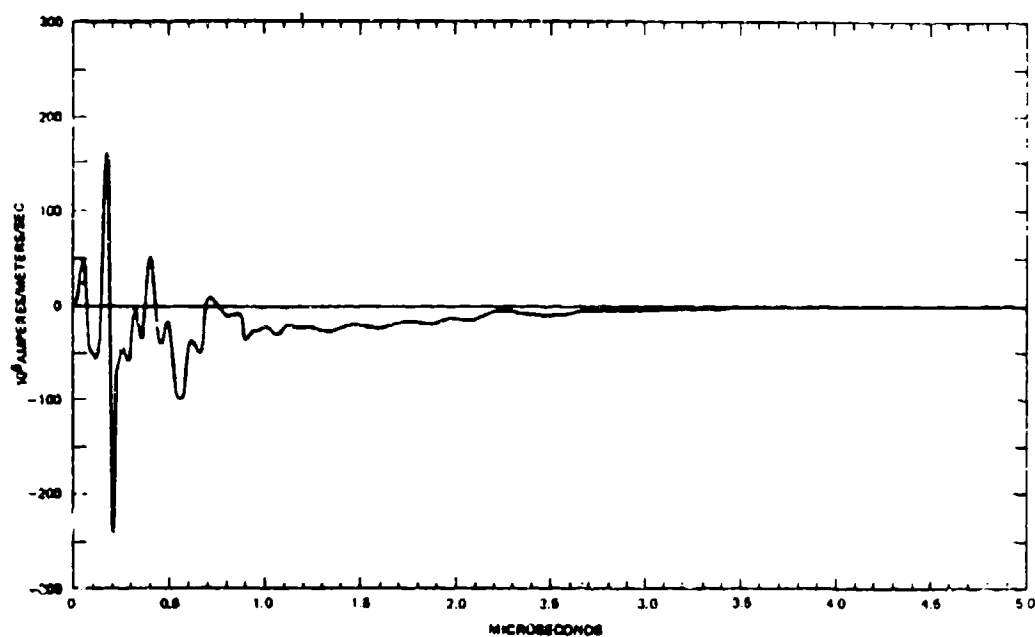Figure 15. Fwd fuselage sensor skin current density (time derivative).
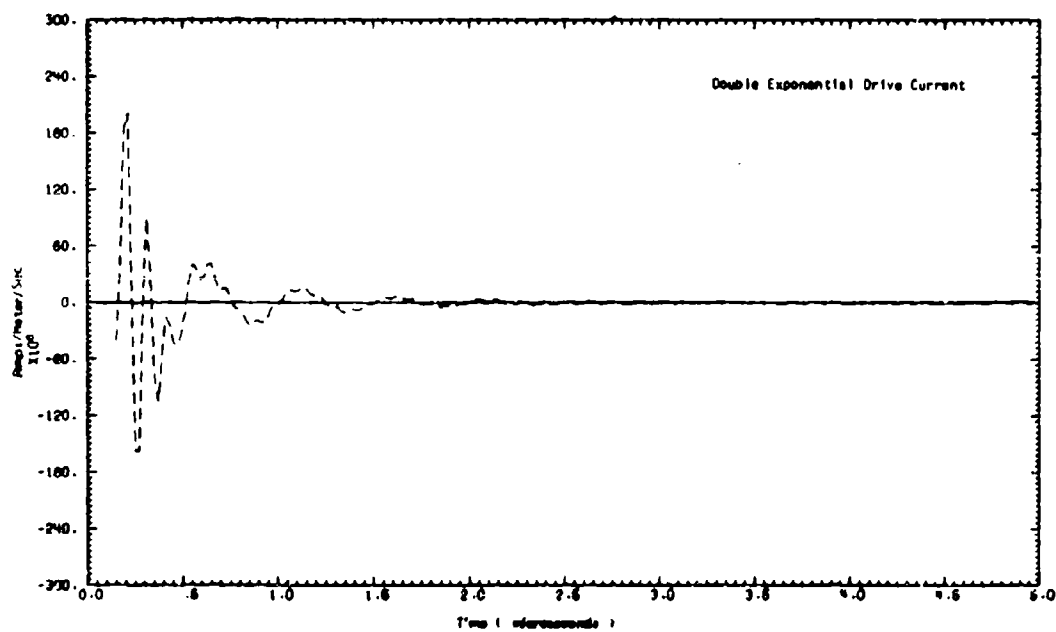
a) Ground test data

b) Calculated response

Figure 16. Aft fuselage sensor skin current density (time derivative).

35

a) Ground test data

b) Calculated response

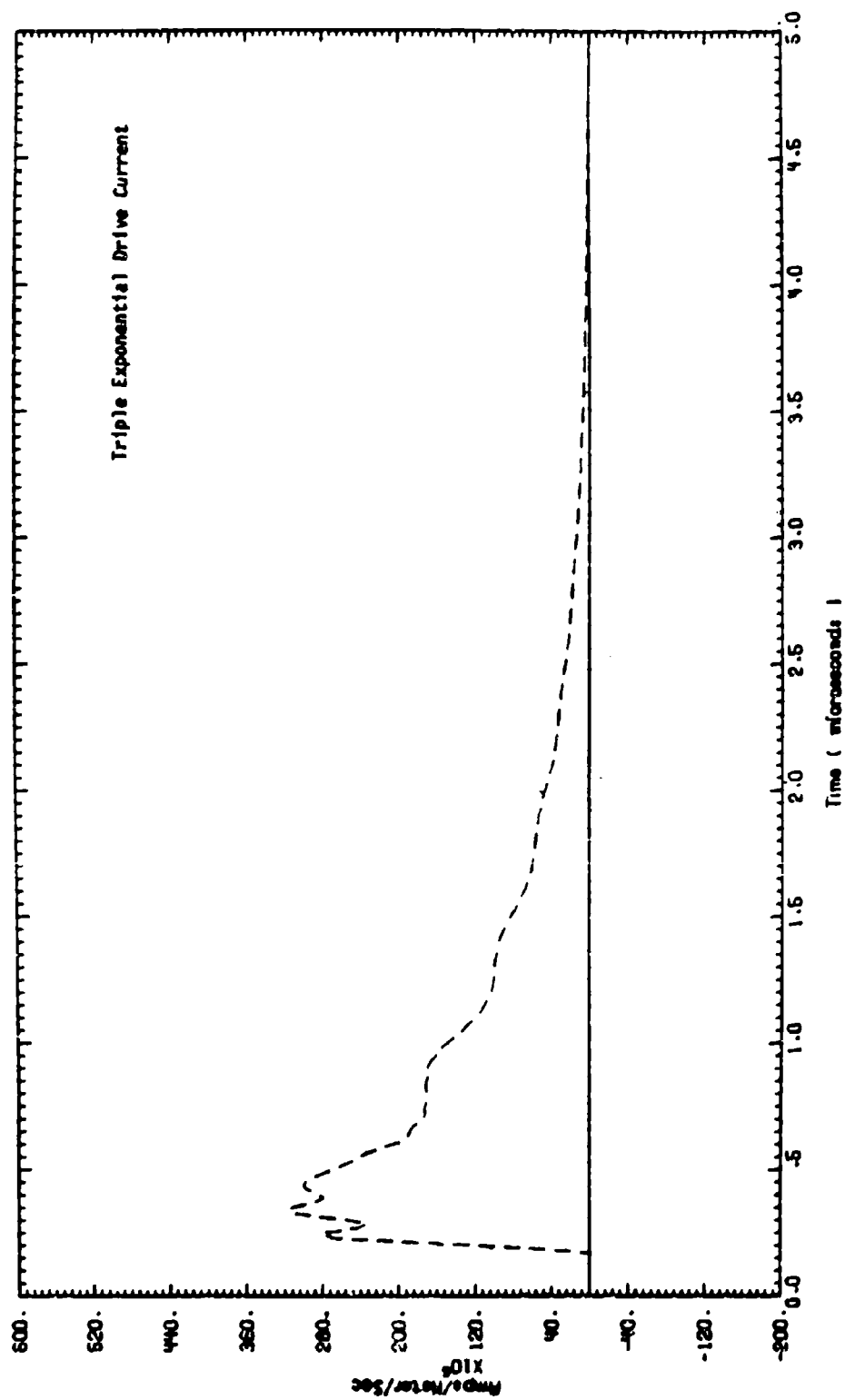Figure 17. Right wing sensor skin current density (time derivative).

Figure 18. Calculated forward fuselage sensor skin current density (time derivative).
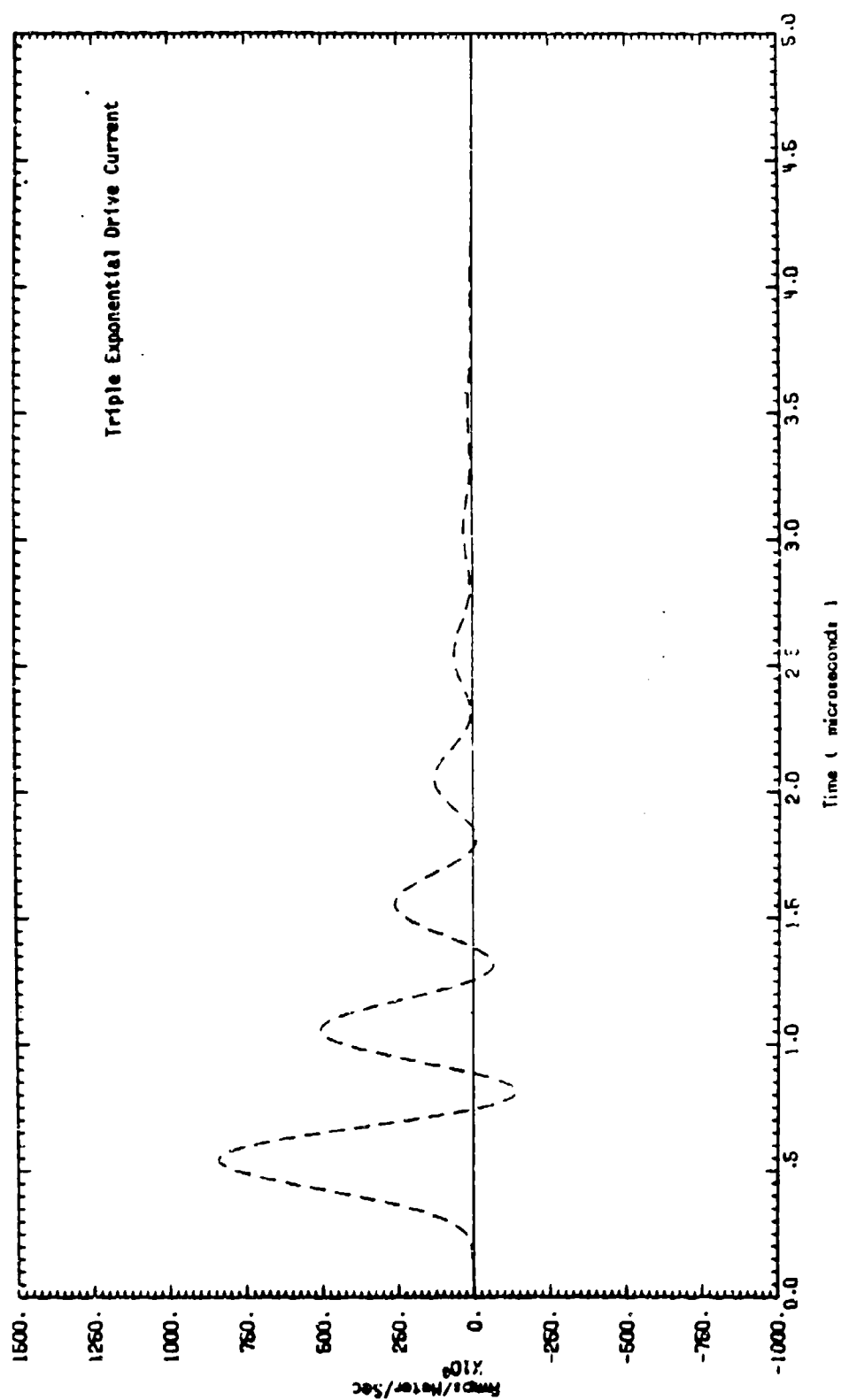
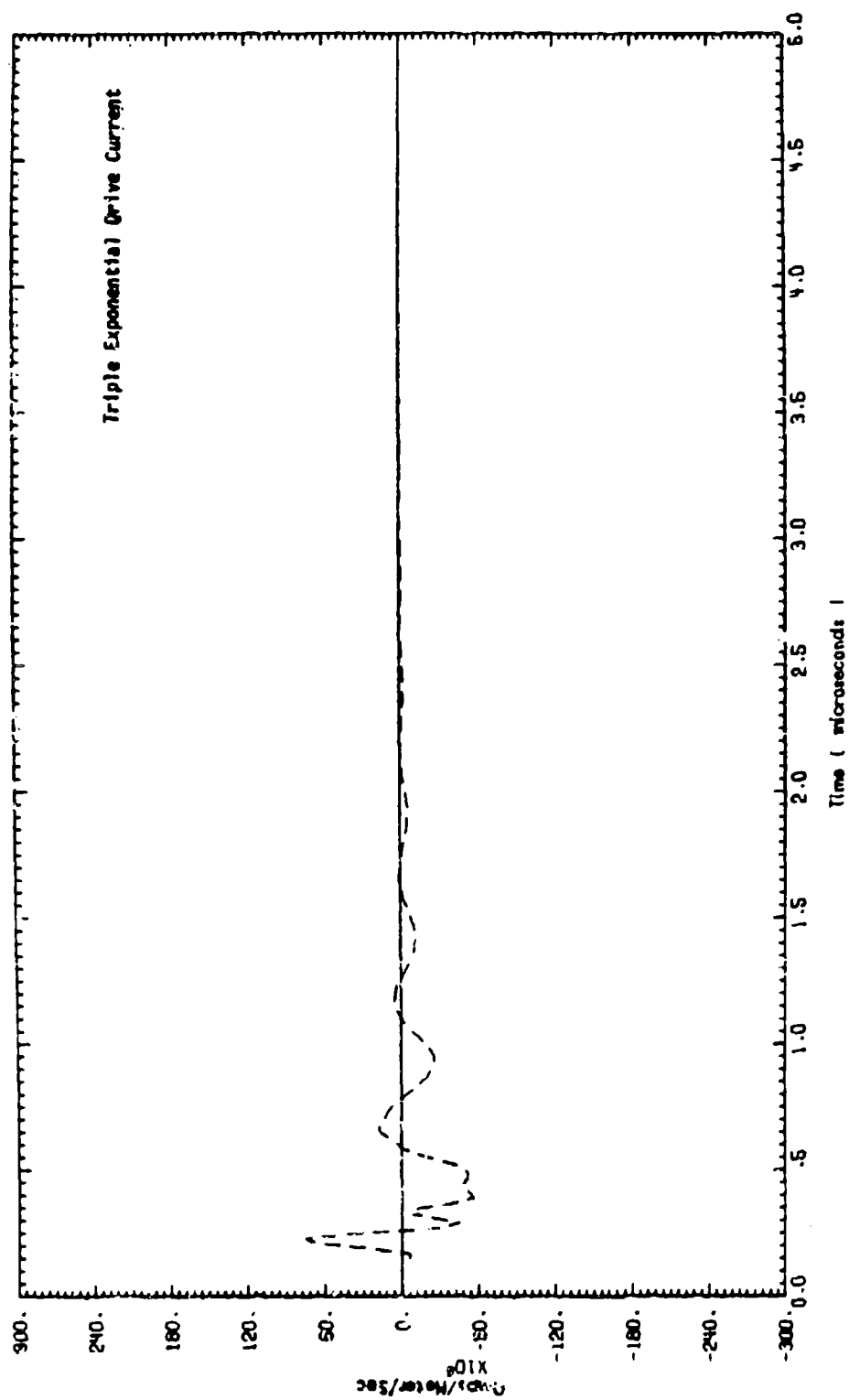Figure 19. Calculated aft body sensor skin current density (time derivative).

Figure 20. Calculated right wing sensor skin current density (time derivative).

The power cart cable current was not measured but the calculated current is displayed in Figures 21 and 22. This power cable system is very important for two reasons. First, the cable adds large amounts of ground capacitance to the fuselage depressing the first aircraft array component resonance to about 2 MHz. It would have been about 4-5 MHz with the cable disconnected. The unperturbed (in-flight or on-ground) first aircraft fuselage resonance is about 10 MHz. The major exterior system resonant frequency has been perturbed by nearly a decade by this simulation geometry. Second, the approximately 30 Amperes of resonant (2 MHz) cable current is conducted directly into the interior power system. Interior measured cabling is tightly coupled to the power system cabling so that all measured responses are dominated by this bogus current.

The agreement in measured and calculated skin current density derivatives can be considered good. It is typical of that which can be expected from wire grid modeling of systems of this degree of complexity where the system geometry has few uncertainties.

The major uncertainties in the external model were ground conductivity and water content and the high frequency pulser drive. The fact that the concrete floor of the hangar and the pad contained no rebar made the ground constituent parameters very important in determining the aircraft response - especially the resonant Q's and ringing times. With rebar, electrical losses and Q's would be set primarily by radiation and secondarily by ohmic losses in array wires and rebar - approximately, Q = 50 at the 2 MHz resonance. With 0.02 mho/meter ground conductivity under an essentially lossless concrete slab, the Q drops to 4-5 due to ground losses; essentially that observed. The conductivity value of σ = .02 was estimated considering the ground to be damp local sand with a fair salt content down to a saltwater table at a depth of 10 feet. It may be noted that this number is essentially the same as for high conductivity midwestern and southern farm land with fair water and nitrate content. Also, it is interesting to note that it is approximately the geometric mean of the conductivities of its constituents: sea water (σ = 4) and sand (σ = 10^{-4}). It is emphasized that this number is merely a reasonable and
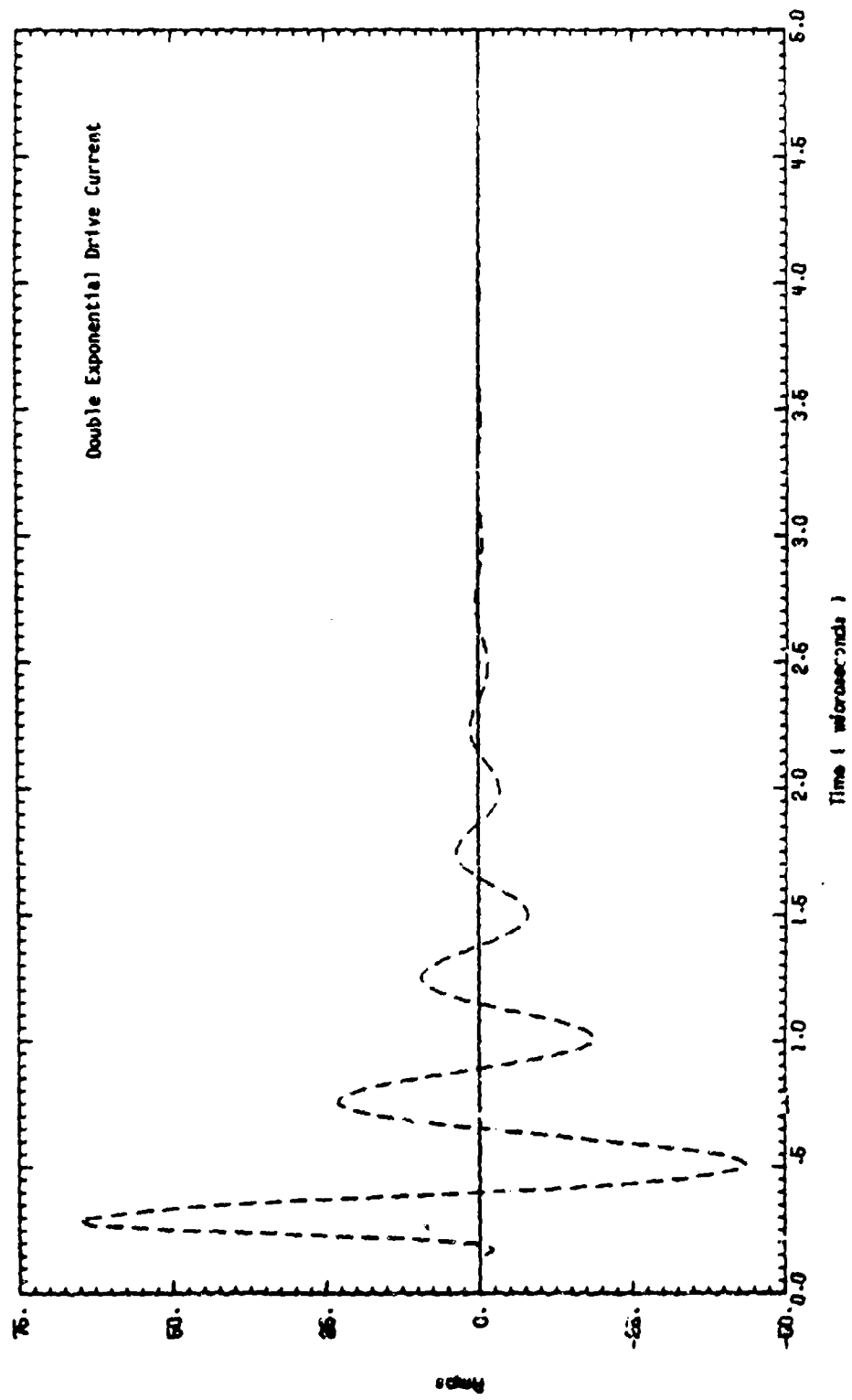
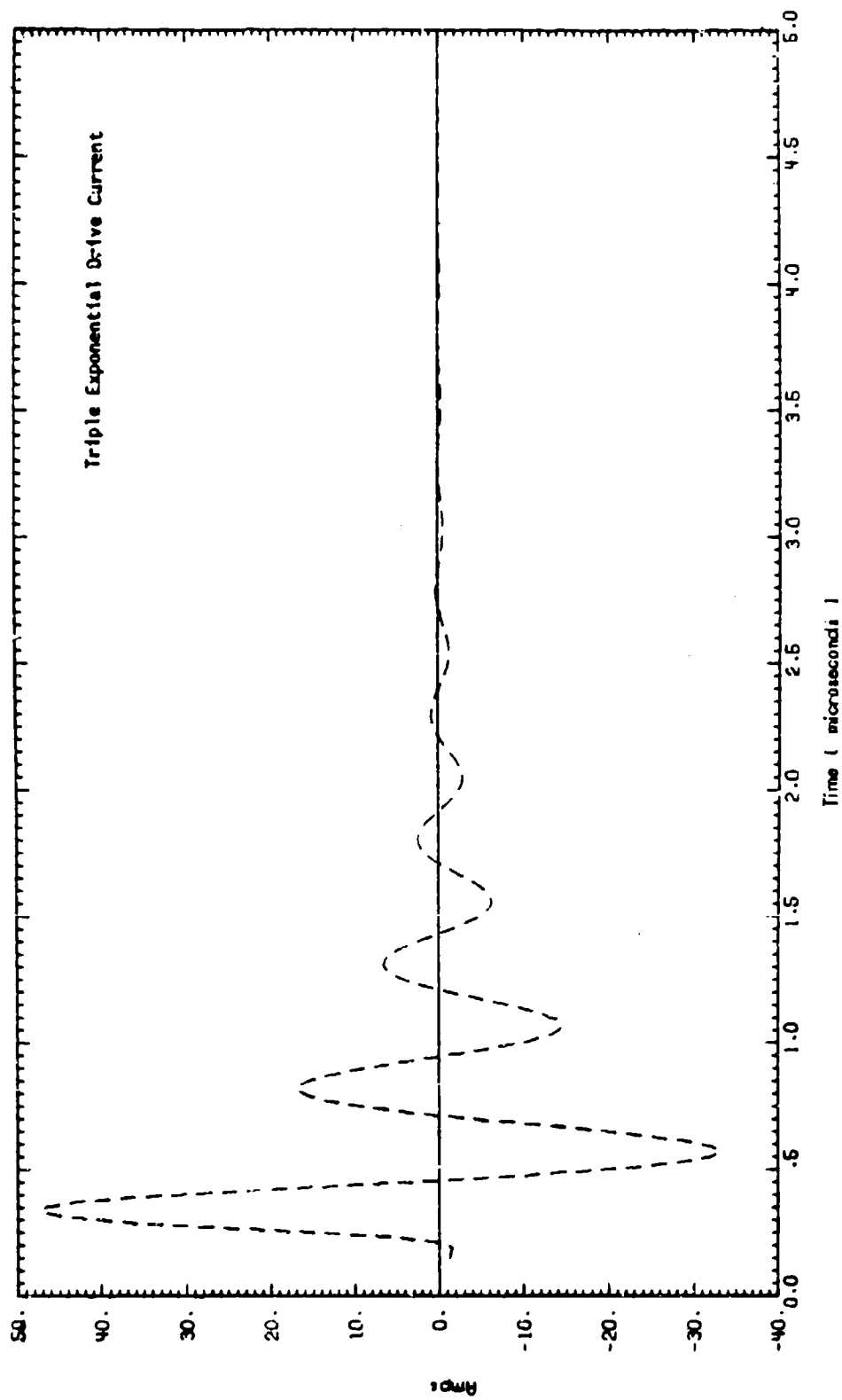Figure 21. Calculated bulk current – external power at cable connector.

Figure 22. Calculated bulk current - external power at cable connector.

fortuitous guess since no ground conductivity data for the site was available. Calculations for the effective ground loss resistance to be added to the wire grid segments follows standard procedures[14,15].

The fine structure of the data can be improved by going to a more complex wire grid model such as the "In-flight" WIRANT model of Figures 3 and 4. This will allow a more realistic distribution of current over the perifery of the wings and fuselage. This would be extremely costly when used with a detailed drive array and pulser model. Many of the essential features of the more detailed solution can be added to the simpler stick model solution by recognizing the current distribution characteristics of the various model constituents of the solution. In particular, the 2 MHz and 10 MHz aircraft-array resonant modes have very different current distributions.

The aft body skin current (derivative) of Figure 16(a) consists primarily of 2 MHz damped sine due to the power cable-aft fuselage resonance riding on a positive offset following the drive current (derivative). The aft body response is well represented by the calculated responses of Figures 16(b) and 19 though subtle differences exist. The dashed part of the measured data (Figure 16(a)) is of uncertain quality and should be ignored. Figure 16(b) represents the unprocessed stick model current with double exponential drive normalized to the local fuselage perimeter. Figure 19 represents a modified model calculation correcting for the surface current distribution of the 2 MHz damped sine current injected onto the fuselage by the power cable near the aft sensor; the triple exponential was used here. The latter curve shows enhancement of the sine term relative to the offset and crosses zero better approximating the measured data.

The wing current density measured at the aft edge of the right wing response (Figure 17(a)) consists primarily of wing-wing and wing-to-nose resonances near 10 MHz, some 2 MHz current charging wing capacitance, and a negative offset following the drive current (derivative) due to the inductive spreading of fuselage current onto and off of the wing near its root.

The offset term does not exist in the basic model solution of Figure 17(b) since the single wing cylinder model can not support the spreading current. This term is added in Figure 20 by adding in a calculated negative fraction of forward fuselage current. Figure 20 also uses the triple exponential drive.

The power cart cable has a bulk current of approximately 60 amperes peak. The calculated responses for double and triple exponential drive are shown in Figures 21 and 22. This response is essentially a damped sine at 2 MHz. No offset terms are present because the cable is an open ended filamentary conductor connected at a single point to the fuselage. One of the two conductors enter the aircraft and attaches directly to the power bus. This produces a Norton source of approximately 30 amperes on the power bus.

The forward belly skin current (derivative) appears in Figure 15. It consists of the same basic terms as the aft belly measurement except that the 2 MHz term is much reduced. This is true because the forward fuselage is merely the feed line for the parallel resonant aft system where aft fuselage and drive array furnish the inductance and the power cable and wings furnish the capacitance. The aft circuit appears to be high impedance at 2 MHz and low impedance below the resonance where the offset term is constituted; this results in little 2 MHz current but an offset current equal to the drive current. It is easily seen that both of the fuselage current terms have an offset term equal to the drive current derivative normalized to the local fuselage perimeter confirming the measurements.

   b.   Interior Responses

Five measured interior responses were available on the layed-in cables at the experimenters rack. They include open circuit voltages and short circuit currents on lines to the right wing, the upper tail, and aft belly field mill on the "hell hole" door (current only). These measured and calculated data are shown in Figures 23 through 37.
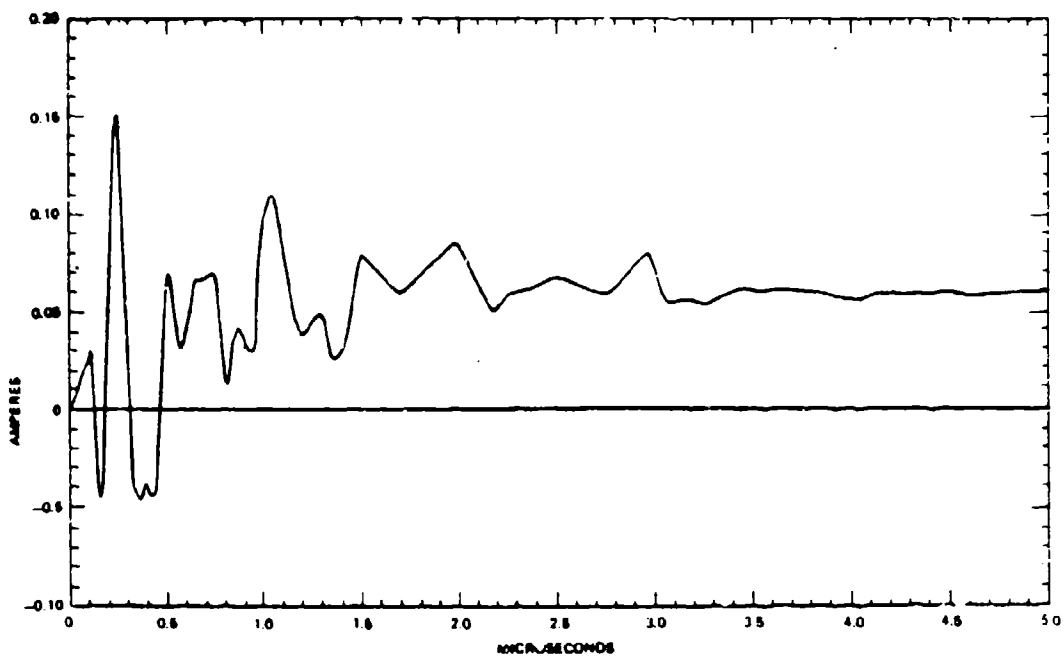
a) Ground test data
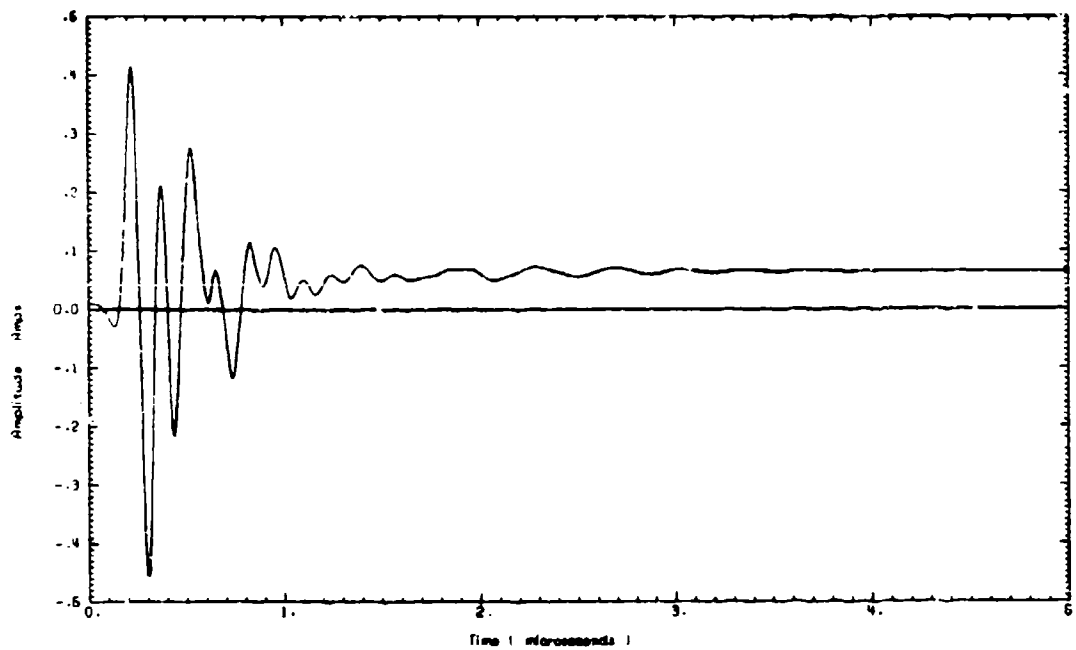
b) Calculated response

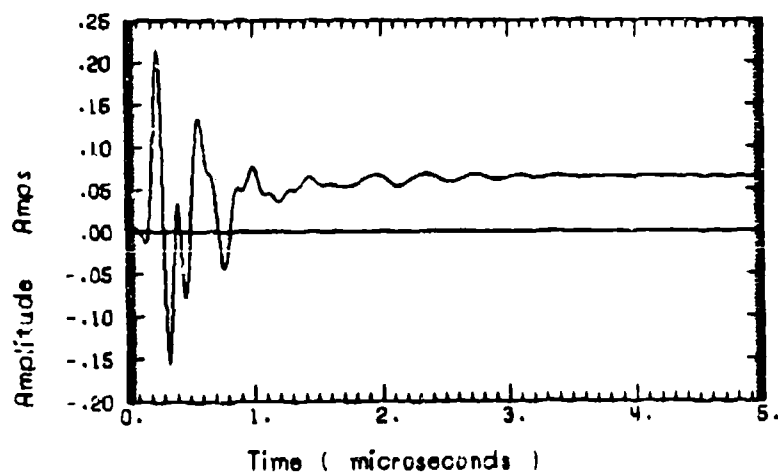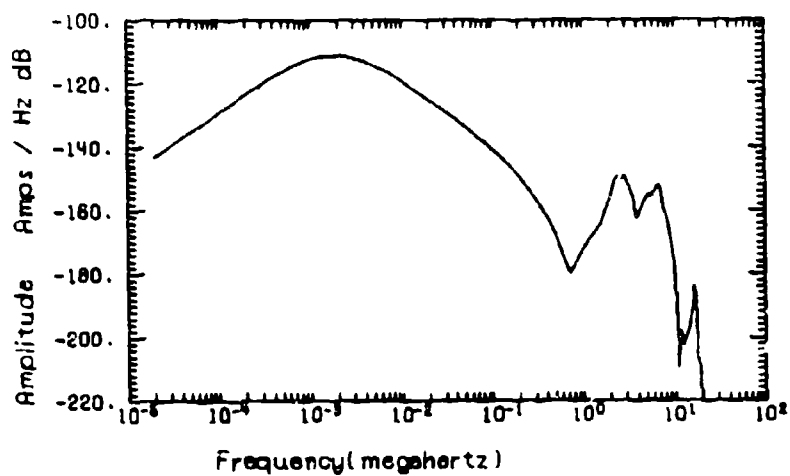Figure 23.   Right wing wire short-circuit current.

45

Figure 24. Calculated right wing wire short-circuit current (triple exponential).
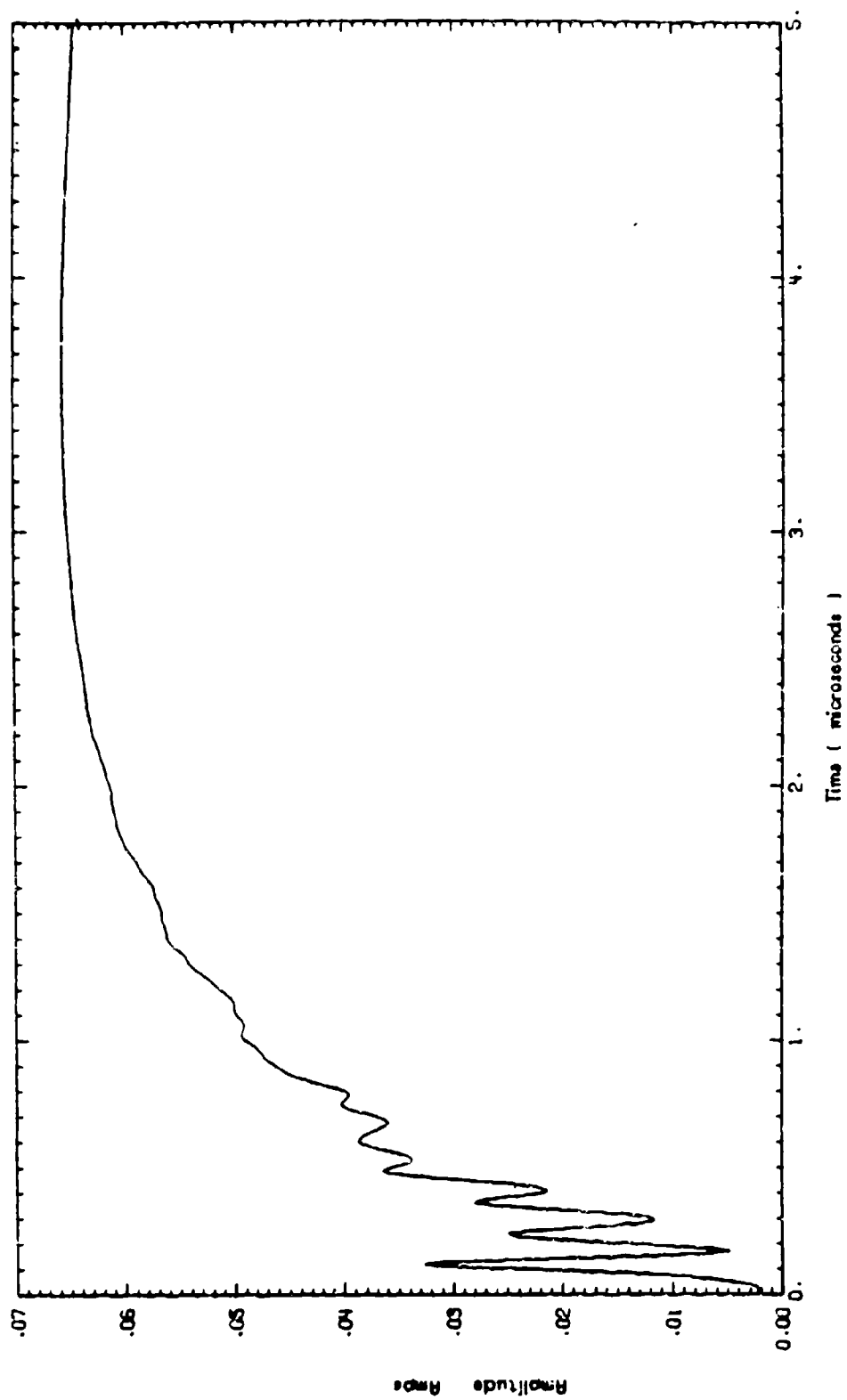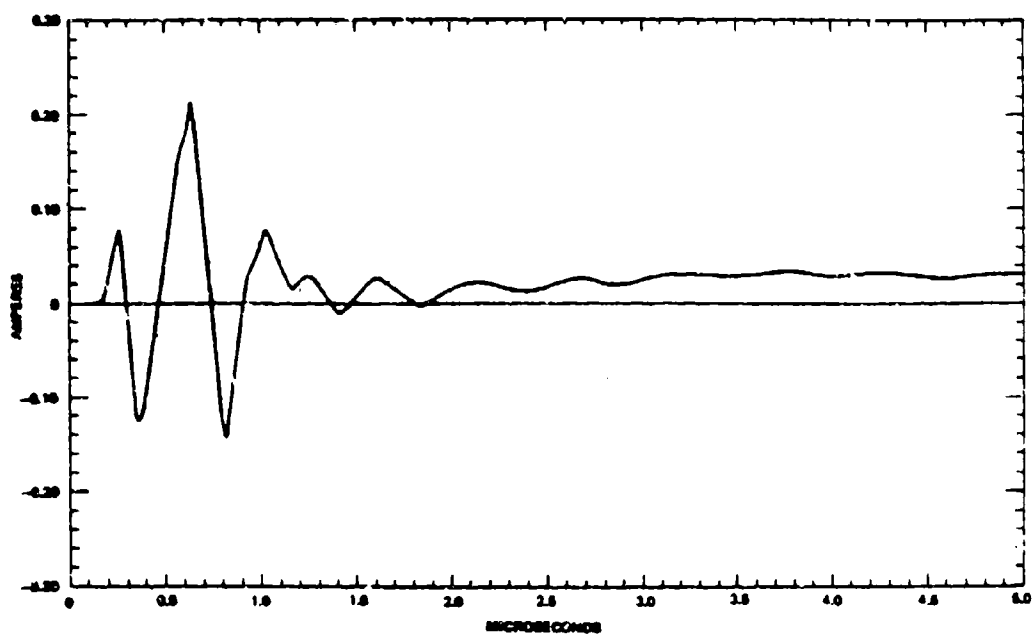
Figure 25. Calculated right wing wire short-circuit current (power cable drive suppressed).

47

a) Ground test data

b) Calculated response

Figure 26. Aft belly wire short-circuit current.

48

Figure 27. Calculated aft belly wire short-circuit current (triple exponential).

49
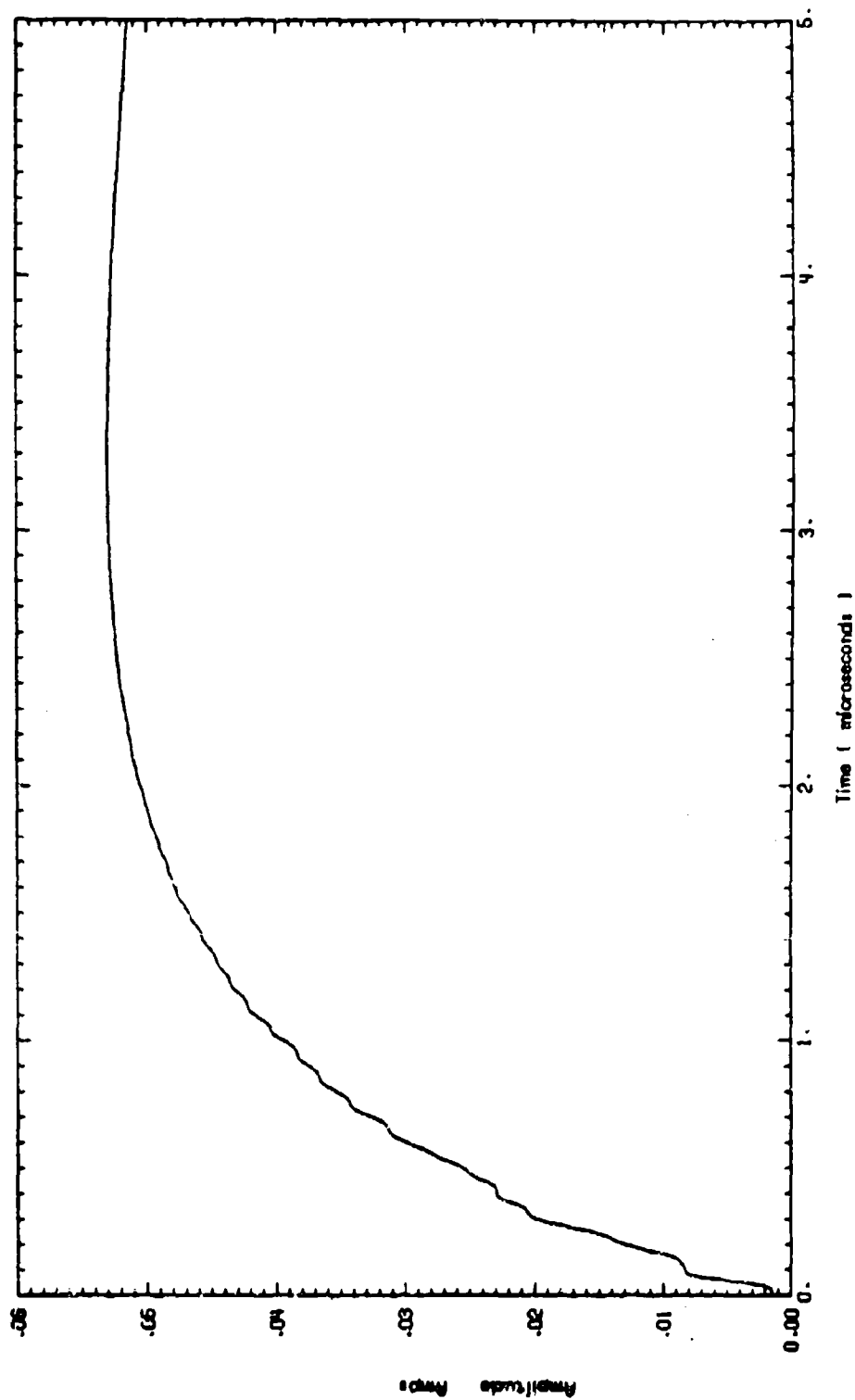
Figure 28. Calculated aft belly wire short-circuit current (power cable drive suppressed).
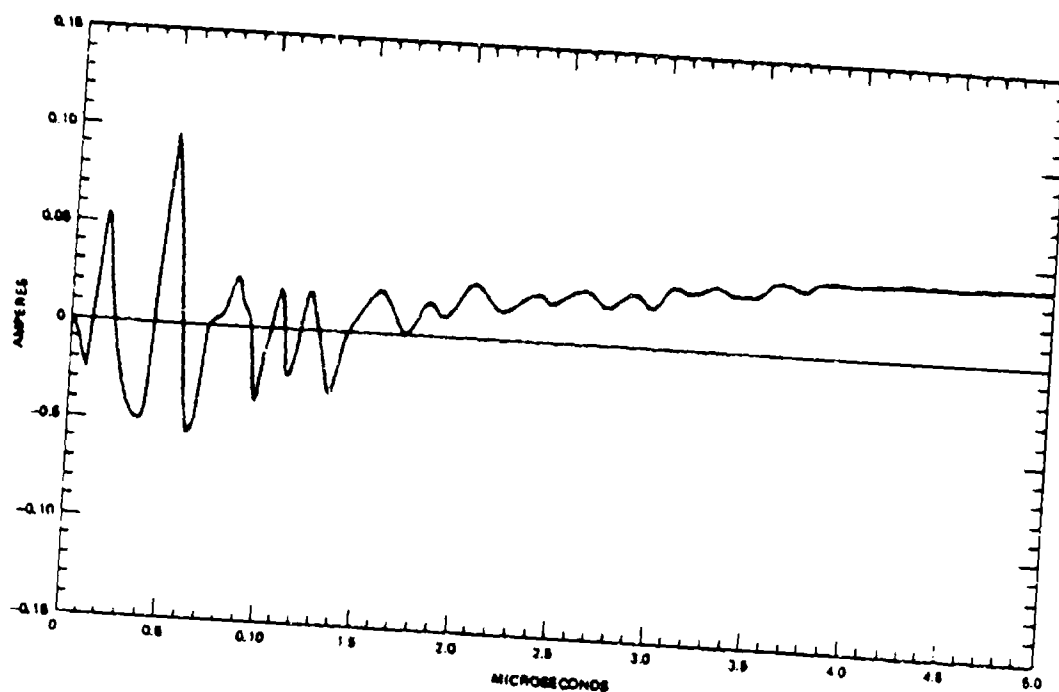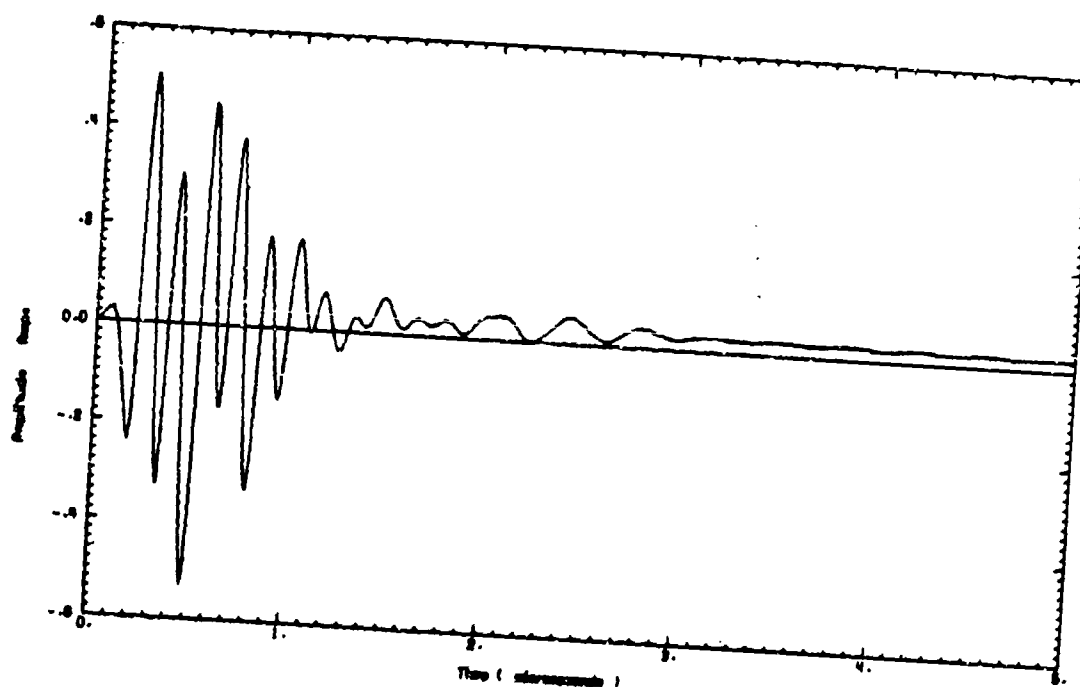
a) Ground test data

b) Calculated response

Figure 29. Tail wire short-circuit current.

51
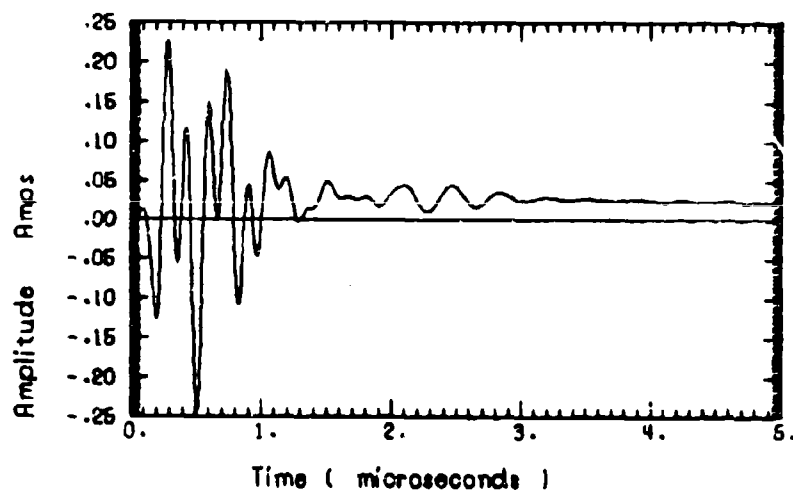
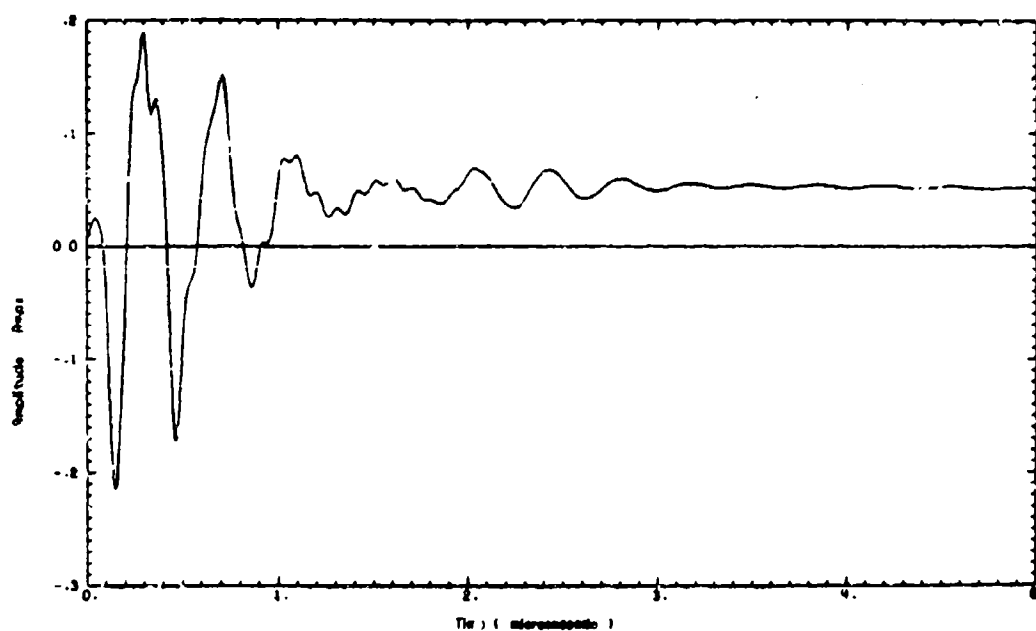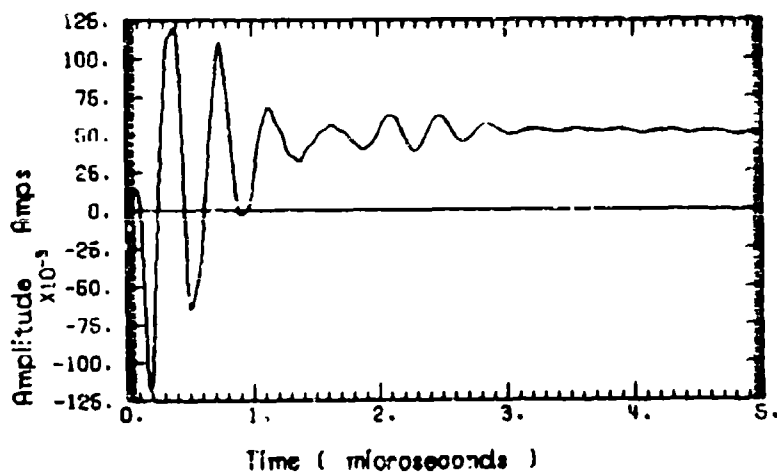Figure 30. Calculated tail wire short-circuit current (triple exponential).
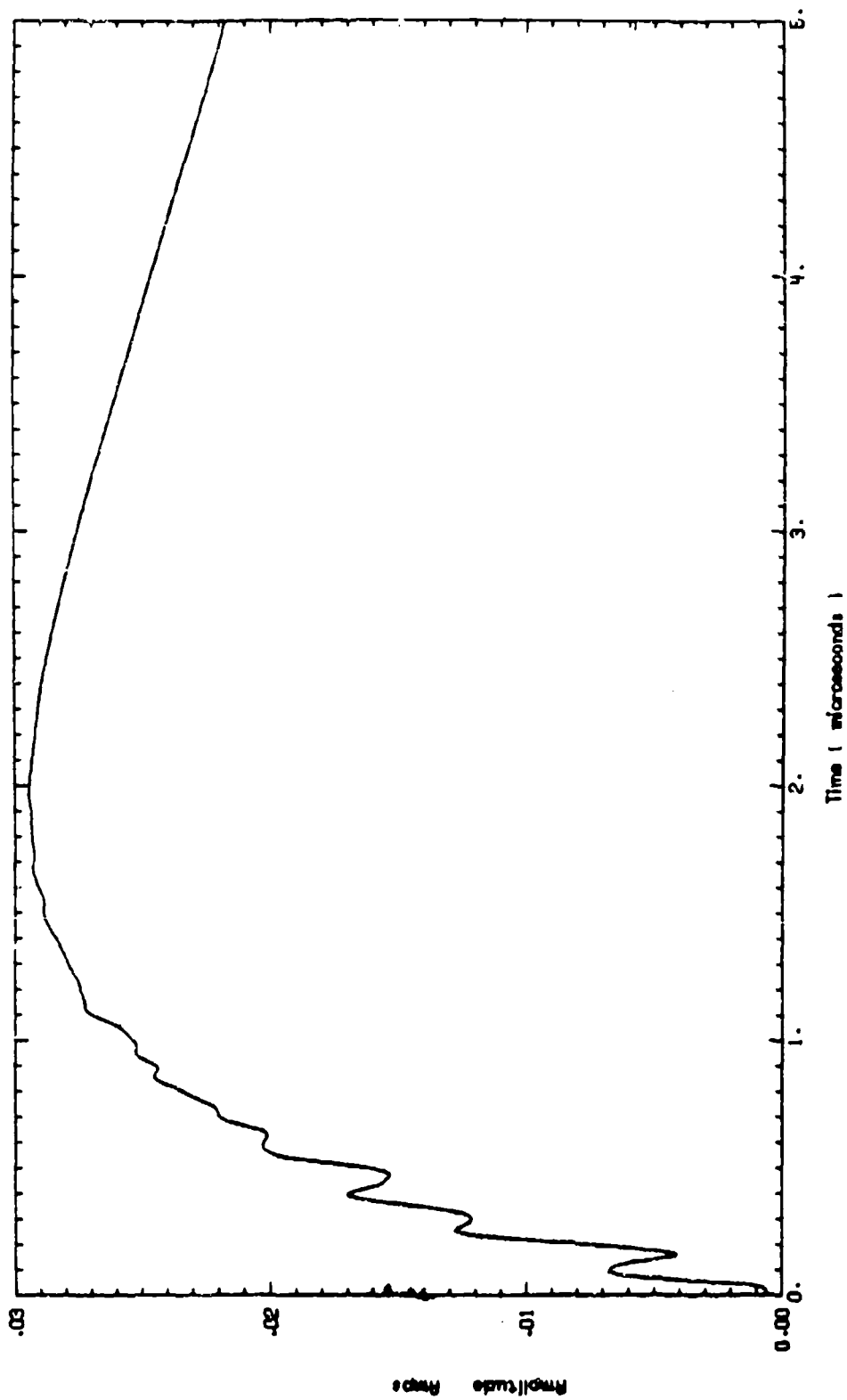
Figure 31. Calculated tail wire short-circuit current (power cable drive suppressed).
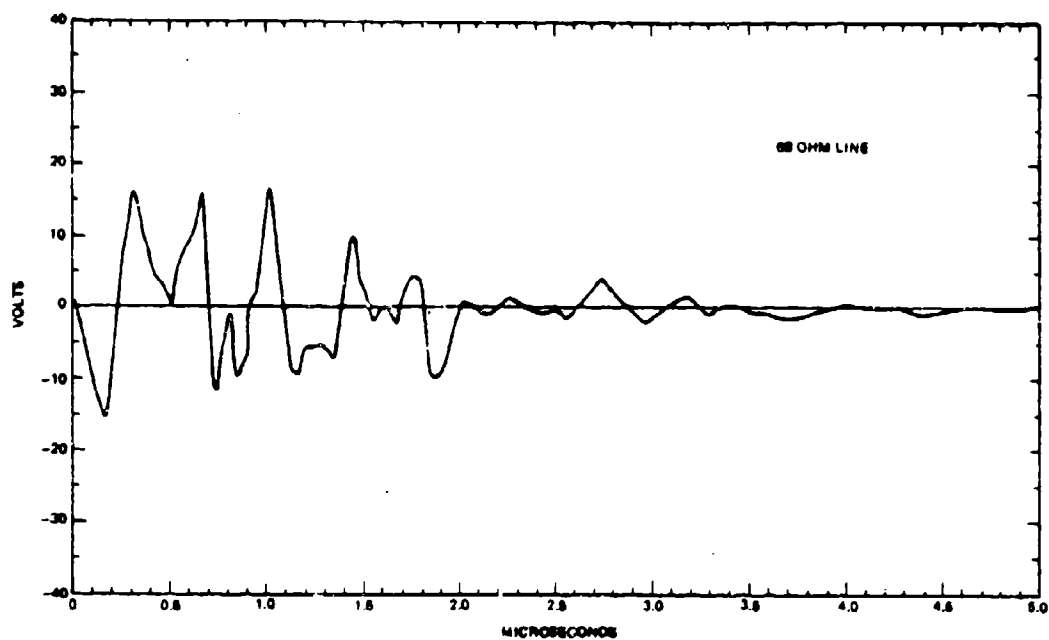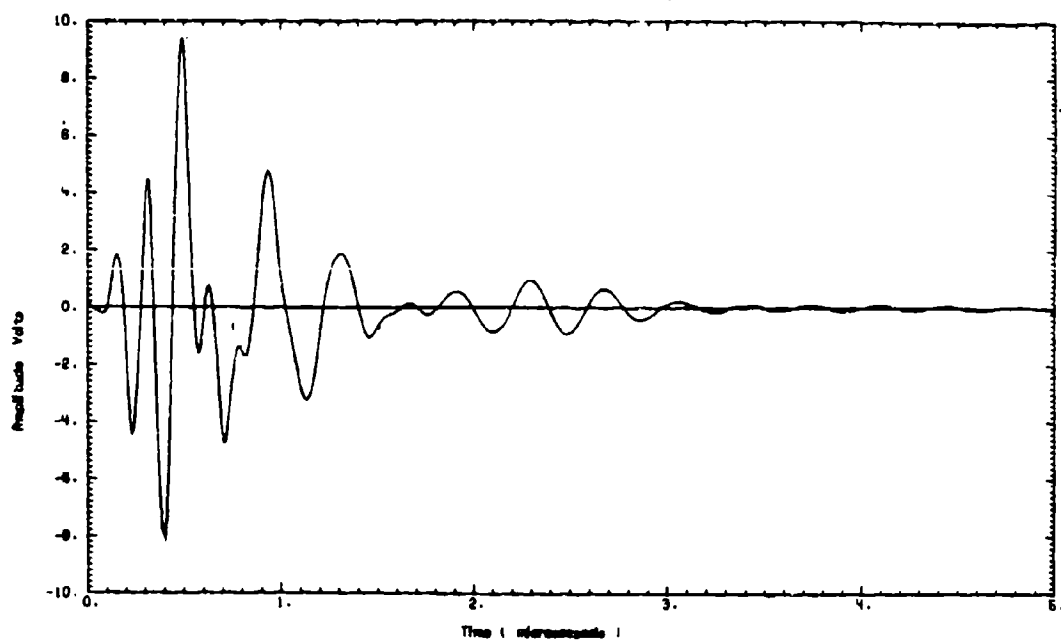
a) Ground test data

b) Calculated response

Figure 32. Right wing wire voltage.

54
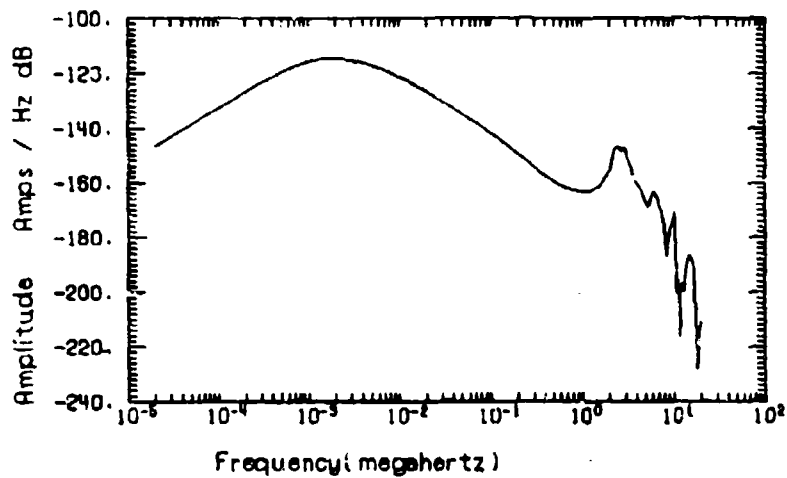
Figure 33.   Calculated right wing wire voltage (triple exponential).

Figure 34. Calculated right wing wire voltage (power cable drive suppressed).
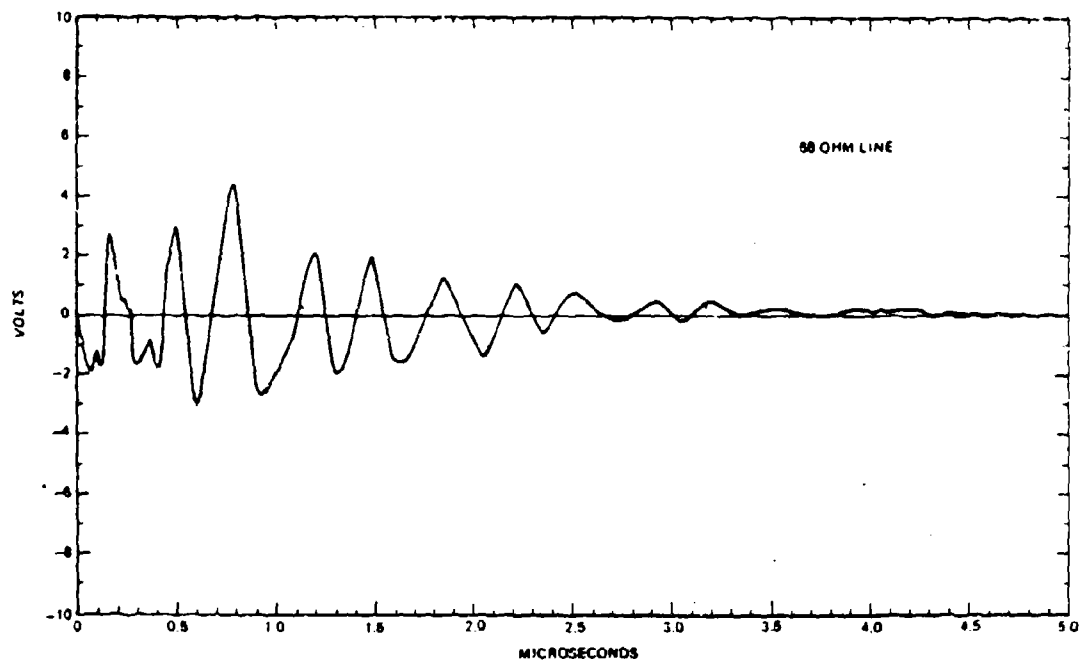
a) Ground test data
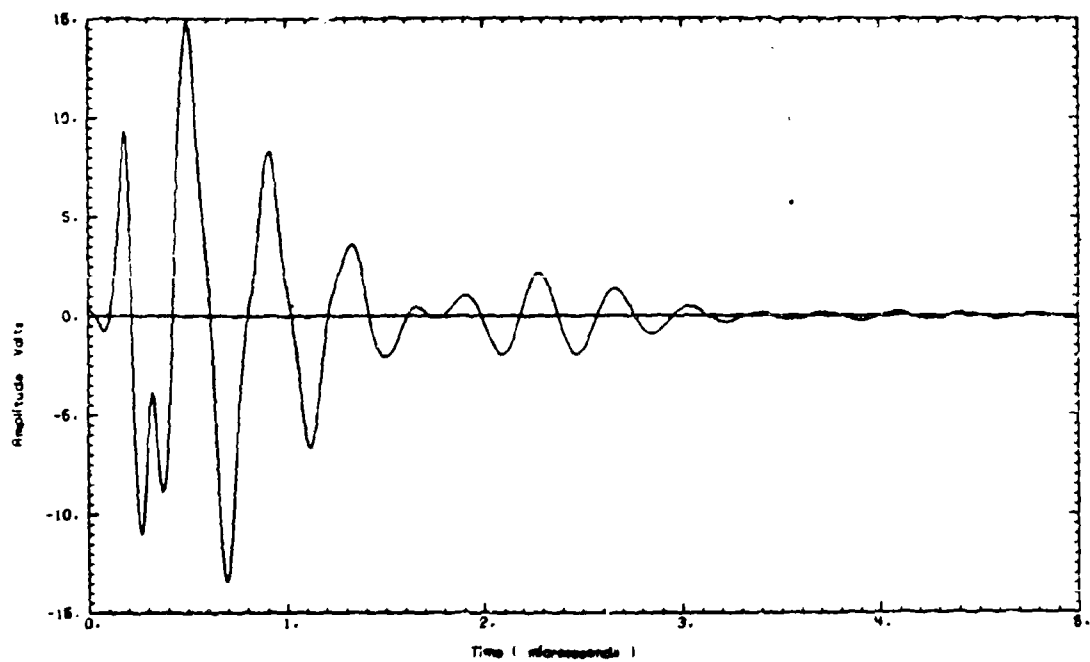
b) Calculated response

Figure 35. Tail wire voltage.

57
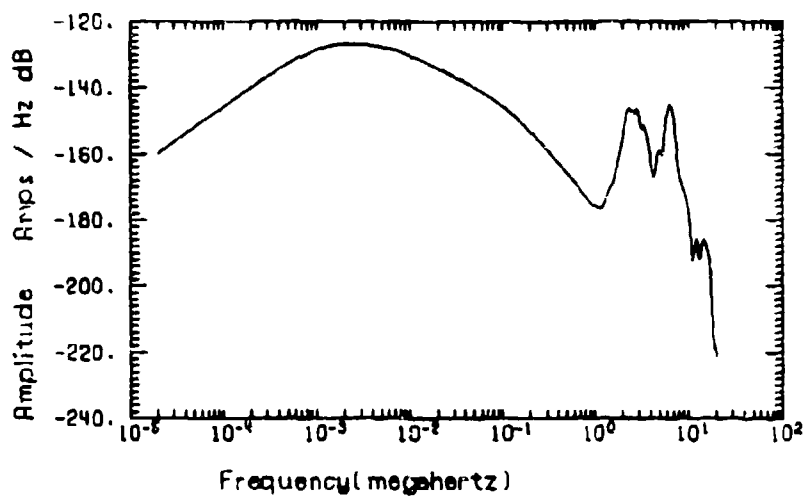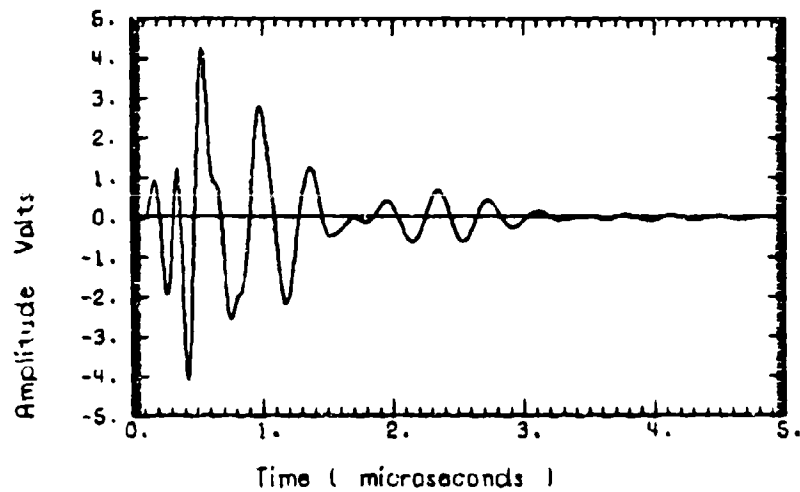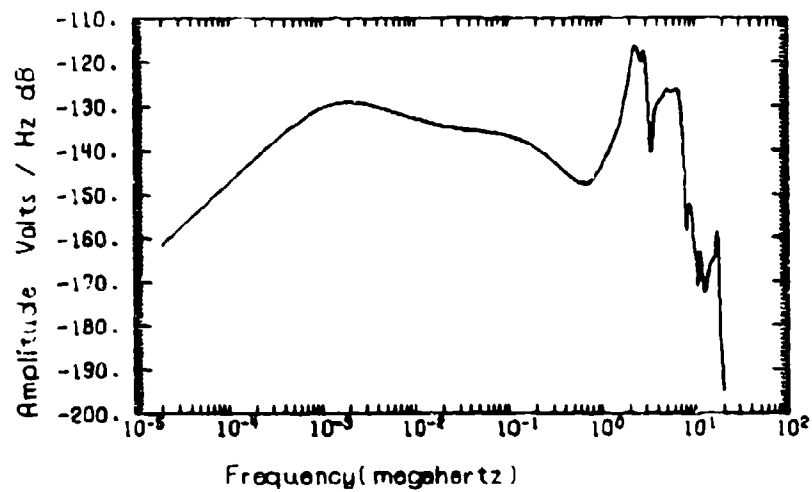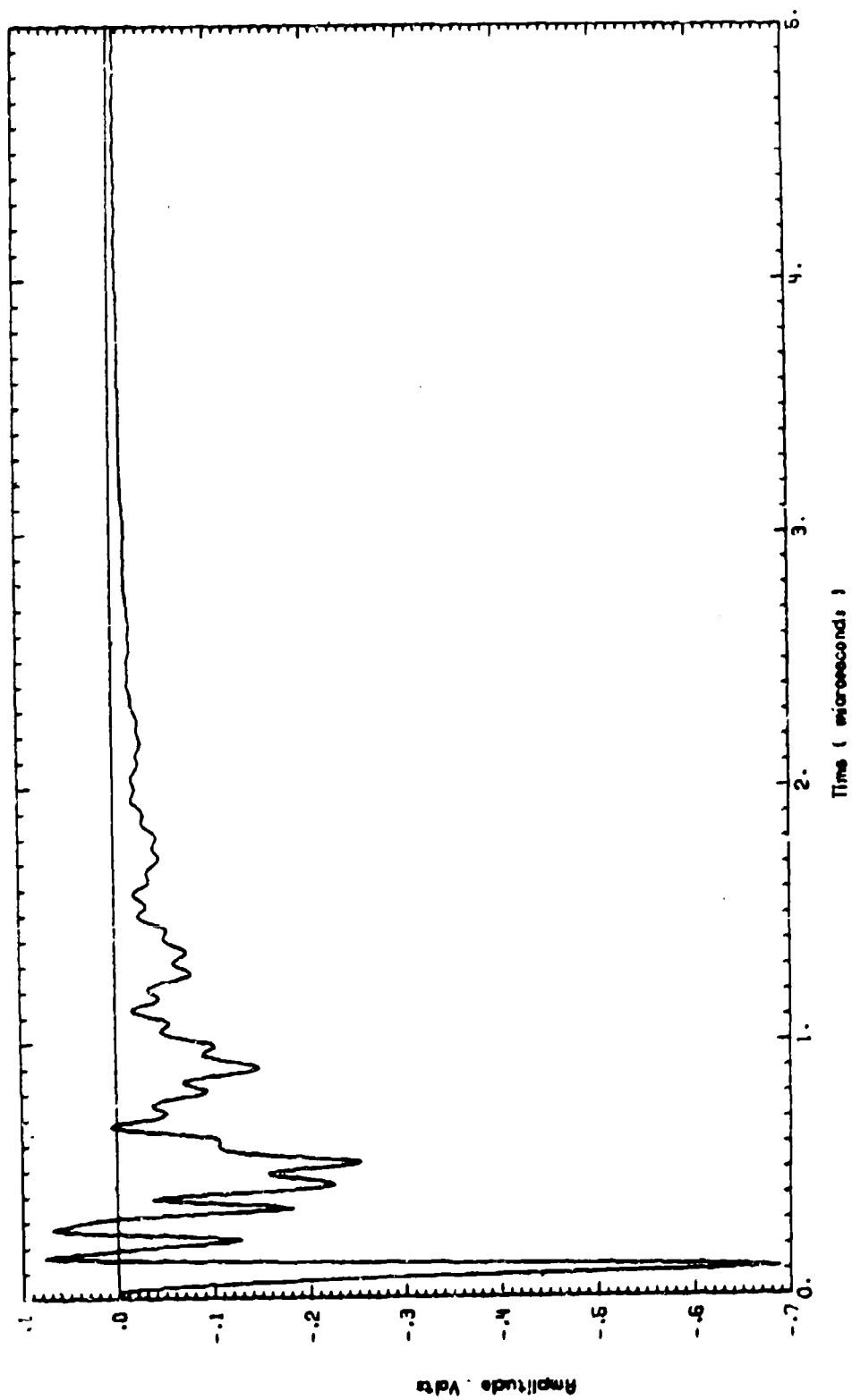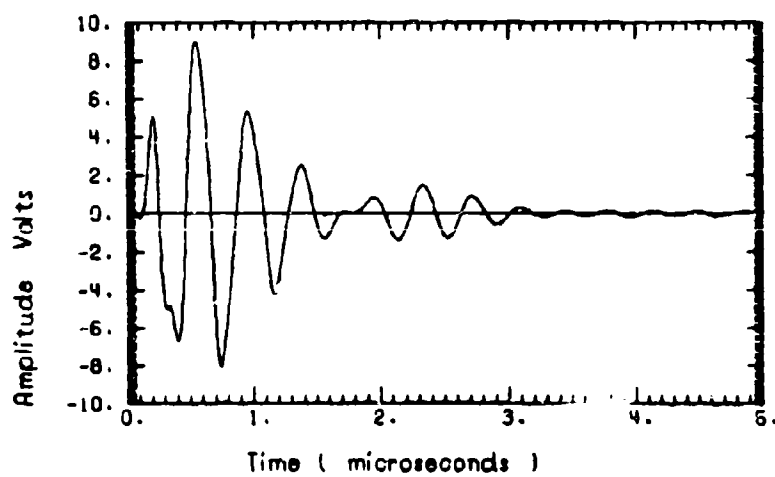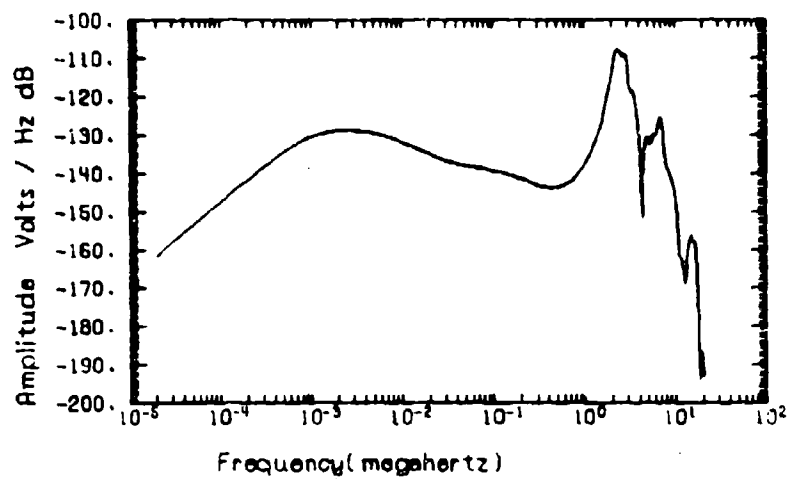
Figure 36. Calculated tail wire voltage (triple exponential).
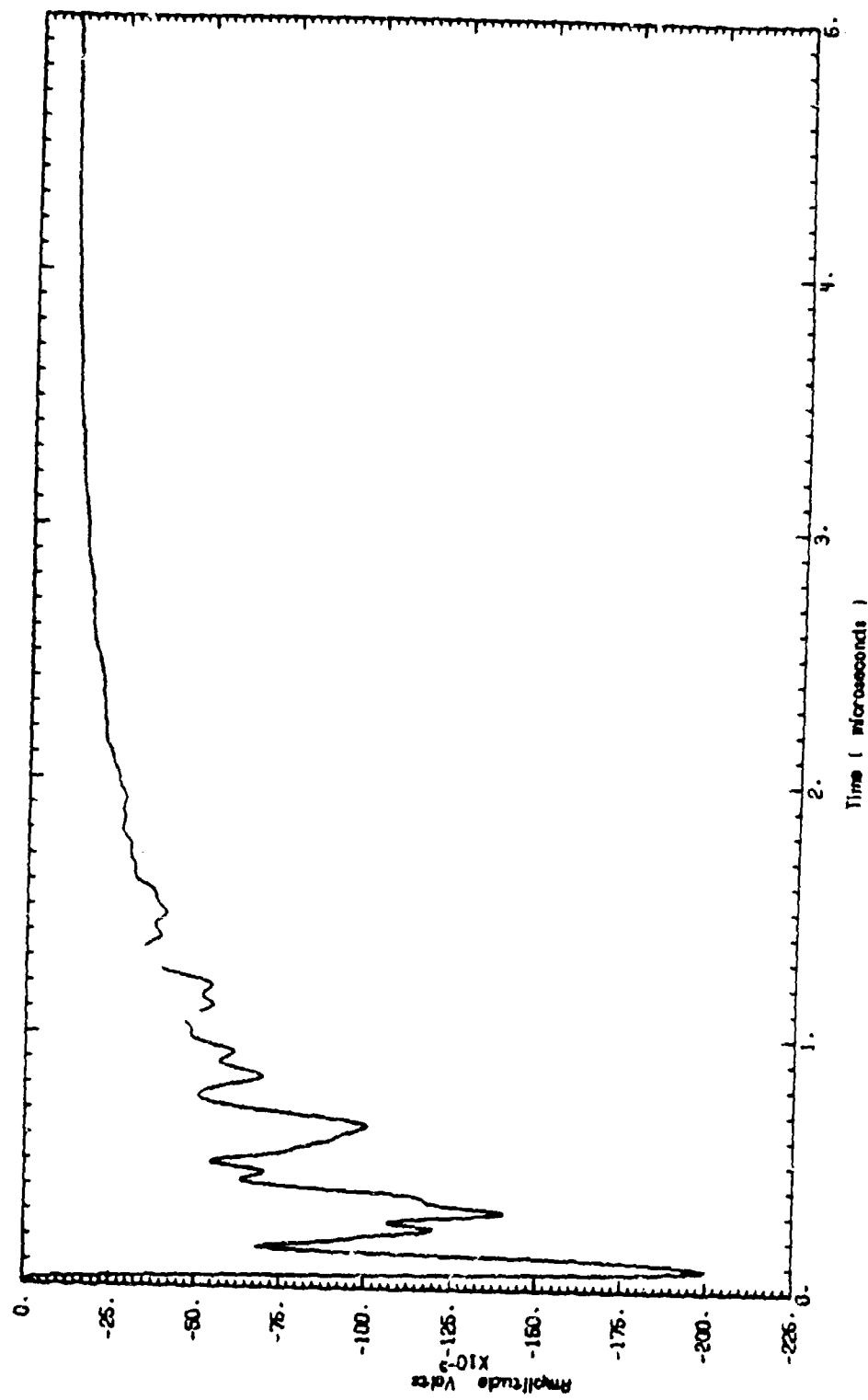
Figure 37. Calculated tail wire voltage (power cable drive suppressed).

All of the short circuit currents have similar form and level. This is not surprising since each of these lines have similar runs, terminations, and the same principal excitation sources. Each is coupled to the power system and receives oscillatory response primarily from it. The oscillatory response is dominated by the 2 MHz external response, the half wavelength resonance of the individual wire involved (7-12 MHz) and quarterwave resonances (3-4 MHz) of the large numbers of cable wires which are open on one end and essentially grounded on the other. These latter cross-couple currents onto the observed lines once driven by the power system.

The currents all show an offset term following the drive current. This results from magnetic coupling through the cabin windows between the forward fuselage current and observed lines. In the later time of the plots and at the lower frequencies which constitute the response there, the observed lines, being shorted at both ends during the measurement, are inductive loops responding nondispersively to the magnetically coupled external current. This can be seen as follows: some of the magnetic field from the external current penetrates the windows and threads the wire loop formed by ground wire ends. The induced voltage is $V = j\omega M \ I_{DRIVE}$. The loop impedance is approximately $Z = j\omega L$ so that the short circuit current becomes

$$I_{sc} = \frac{V}{Z} = \frac{j\omega M \ I_{DRIVE}}{j\omega L} = \frac{M}{L} \ I_{DRIVE}$$

The aft belly wire short circuit current is more heavily dominated by the 2 MHz power cable current due to greater exposure along its run to the "hell hole" door area where the power cable enters.

The voltage responses do not show tails (offsets) since they were measured on lines terminated in 68 and 50 ohms (instrumentation). For these, the power system is the only significant source. The primary resonances observed are due to the 2 MHz external resonance and quarterwave cable resonances (3-4 MHz).

60

The measured and calculated responses show the same major
frequency constituents although not precisely in the same amplitude
proportions. The calculated currents tend to be high, 6-10 dB, in their
half wave wire resonance responses due to overcoupling and mode degeneracy
in the interior cable model. The form of the cable model used was such
that all wires within a given cable bundle section were equally coupled to
every other. This was not precisely the case (hence model overcoupling)
in reality. Also, model simplifications included large numbers of parallel
wires reduced to a single equivalent wire to reduce model conductor number
and matrix order. This does not allow the proper splitting of cable mode
resonances and the effective loss and decoupling which results. A more
detailed model would have improved the calculations. Calculated voltage
responses also show the effect of model simplification.

To illustrate the importance of the HF spectral content of the
drive, each measured response is shown with the calculated counterpart for
the double and triple exponential drive currents previously given in
Figure 11.

The dominance of the power system conducted signal is demonstrated
for each interior response by suppressing the power cable Norton current
source in the internal model. This would be the result of filtering the
incoming power cable from the power cart. If the power cart had not been
used, yet another result would have been obtained since the 2 MHz resonance
would have moved up to approximately 5 MHz.

6. LIGHTNING RESPONSE PREDICTIONS

The external cable model developed for the ground test configuration
was used to predict responses due to directly attached and nearby lightning
in an in-flight environment. As described in Section II, the lightning
current assumed was Pierce's[16] 20 kA nominal return stroke current with
1.5 and 40 μs time to peak and half values, respectively. The direct attach
geometry includes attachment points at nose and right wing tip. The nearby
environment assumes a vertical discharge column off the left wing tip at
distance of 100 meters to the aircraft center. This distance seemed a
reasonable "worst-case" range since the probability of closer discharges
not involving actual aircraft attachment seemed small.

In the direct attach case, unlike the ground test, large lightning
currents flow on the wing as well as the forward fuselage. The coupling of
wing current to the wing cable is much stronger than coupling via the cabin
windows to fuselage current. In consequence, as can be seen from Figures 38
and 39, the wing wires show much greater response than the tail wire which
is excited only by the cabin window. The wing response is dominated by
terms following the lightning current (I_{sc}) and its derivative (V_{oc}). The
tail wire responses contain the same constituents (though more than a decade
smaller) but also contain relatively larger proportions of HF cable resonant
components due to preferential cross coupling to the hotter wing wires.

The response of the right wing wires to nearby lightning is shown in
Figure 40. In this geometry the external fields are approximately two orders
of magnitude smaller than in the direct attach case because of the range factor.
Also, in this case, the incident electric field (radial) is directed along the
wings. The peak value of this field is approximately 40 kV/M. It excites
the external resonance and drives the wings capacitively below the resonance.
The incident H field follows the lightning current and induces external differential
mode currents and wire short circuit currents which do the same. The field
configuration enhances the HF resonances of the aircraft over the differential

62

modes, in turn, increasing the relative level of the resonant responses of the cable itself compared to the current and current derivative terms.

The conclusion to be drawn from these curves are that nominal lightning can be a serious threat to aircraft when directly attached. Nearby lightning, if severe (100-200 kA with peak rise times under 1 usec) may cause circuit upset but is not likely to cause circuit damage.
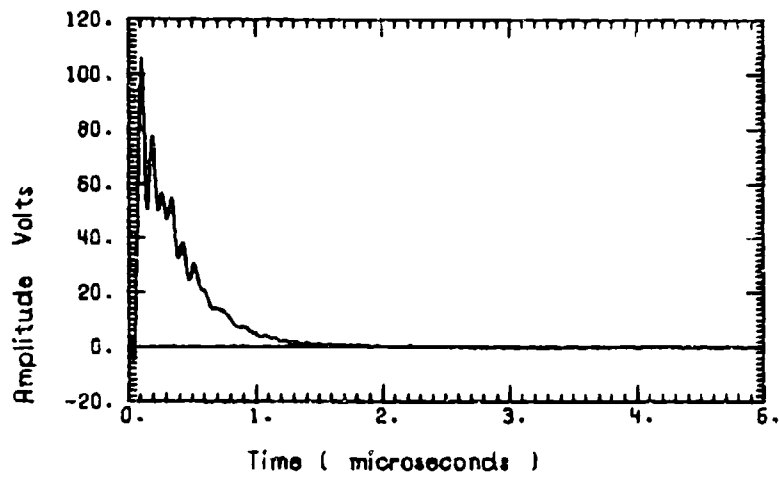
a) Open circuit voltage
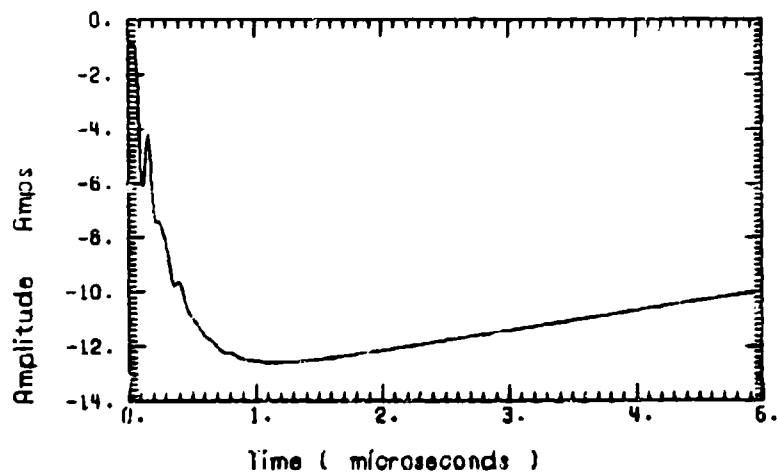
b) Short circuit current

Figure 38. Attached lightning-right wing wire response.

64
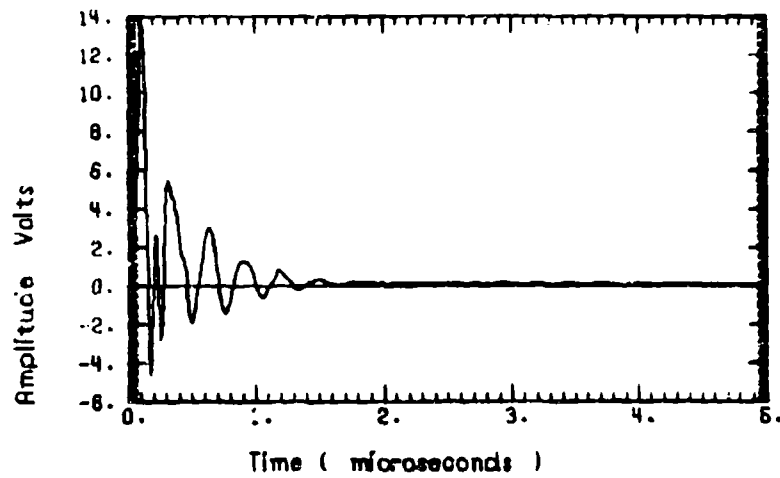
a) Open circuit voltage

b) Short circuit current

Figure 39. Attached lightning—tail wire response.
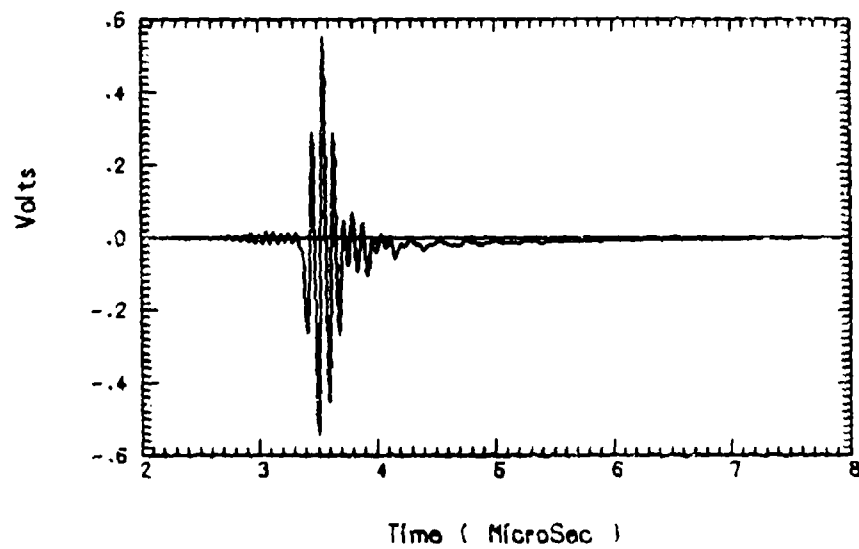
a) Open circuit voltage
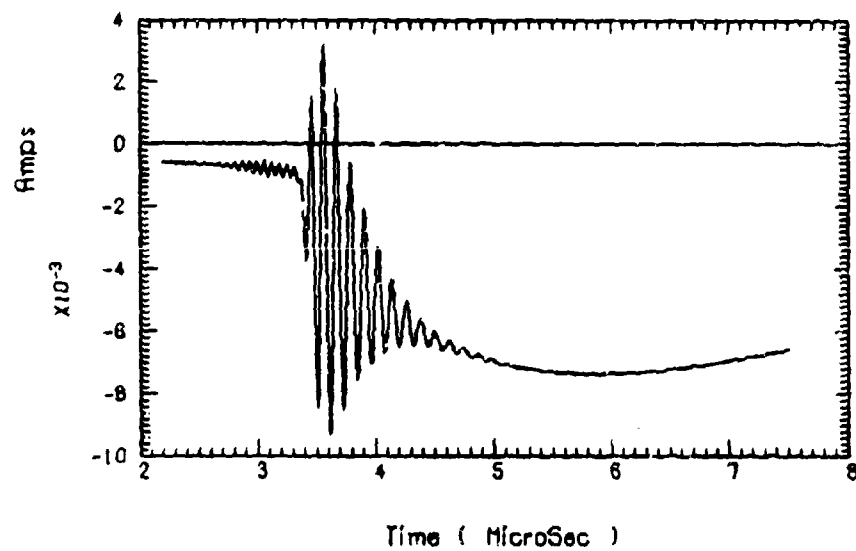
b) Short circuit current

Figure 40. Nearby lightning—right wing wire response.

66

SECTION IV
CONCLUSIONS AND RECOMMENDATIONS

A detailed discussion of the ground test configuration and the nature of the resulting exterior and interior responses as well as their calculated counterparts has been given in earlier sections. The most significant conclusions are listed here.

1) The configuration of the aircraft, drive array, and pulser (Figure 9) altered the aircraft resonant response significantly - with or without an external power cart. Natural aircraft resonances (in-flight or over ground) approximate 10 MHz. With the drive array and without the power cart the first resonance drops to approximately 5 MHz. With the power cart (ungrounded), it drops to the observed 2 MHz.

2) Principal internal cable resonances fall in the 3 to 12 MHz range. If an external resonance falls on (or near) an internal cable resonance, internal responses increase greatly. Simulation of the proper natural external resonant frequencies is important if the resulting time domain data is to be extrapolated to some environmental criteria level.

3) The power cart capacitance tunes the external aircraft to resonance at 2 MHz and injects half its current (30 amperes) into the interior power system. This current couples to the measured cables and dominates other sources in measured/ calculated responses by 30 or more dB in the HF range. This precludes use of the measured data for extrapolation to lightning criteria since normal penetration sources are obscured by a bogus source.

67

4) The drive current injected into the array at the pulser is required for data extrapolation. Actually, two lines over ground connect the pulser to the array system and the large pulser capacitors have a fairly large ground capacitance. At HF frequencies it is necessary to measure (specify) the currents in both leads since both common and differential modes can exist on the two wire feed line. Only one line current was measured; consequently, only this current was enforced on the model resulting in some high frequency model error.

5) The measured drive current was given as two "scope" photos with 2.5 and 25 microseconds (µs) per division. This allows resolution of the resultant HF spectrum to about 1-2 MHz. As shown in Figure 11, it leaves very substantial ambiguity in the drive spectrum above 2 MHz. Since, for this size of aircraft, exterior natural resonances approximate 10 MHz and interior resonances span 3-12 MHz, the resolution of these photos is inadequate. 0.5 µs/div. is appropriate here.

6) The fact that the power system became the principle cable drive mechanism, by cross coupling to power (cart) cable conducted currents, greatly complicated the modeling effort. When the measured cables receive the same drive as all others (cabin window and wing spar field penetration, for example) the modeling is simplified. Each measured cable can be modeled essentially separately with an empirically based common mode bundle model used to account for the loading effects of adjacent cable conductors. This assumption is the physical basis of the efficient and economical SINGLIN code[18]. When the source is cross coupling to a "hot" cable system the process is greatly complicated since the entire cable system must be precisely modeled so that the

voltages and currents on the "hot" cable system can be accurately determined over the entire active run in common with the measured cables. In this case, the modeling effort and model size were increased by more than an order of magnitude.

7) The absence of a ground screen or rebar in the concrete floor greatly affected the Q of the 2 MHz system resonance. Over a ground screen, it would have been approximately 50 due to reduced radiation at the low resonant frequency. A ground conductivity of 0.02 mhos/meter was assumed based upon ground conductivity maps and a limited knowledge of the area. Calculated ground losses were added to the model based upon the above conductivity yielding essentially the observed (measured) Q of 4-5.

8) Agreement between measured and calculated external skin currents is good, particularly, after correction for model current distributions not calculated by the stick model.

9) Agreement for internal responses is acceptable and representative of that normally obtained for systems of this complexity. All major resonant and tail (offset) responses were present in the model calculations. The levels of these constituent terms can be "improved" by increasing the complexity (and cost) of the internal model.

Recommendations for future tests include:

1) Use of on-board battery power to avoid perturbing effects of external power cables.

2) Selection of a simulation geometry to maintain the frequency and Q of the most significant external resonances.

3) Selection of drive current waveforms. When the goal is determination of interior cable response to attached lightning, the HF spectrum is most important and, therefore, the drive current time derivative at time zero (for double exponential or damped sine currents) is the important parameter to set, not peak current.

A geometrical configuration which tends to maintain the basic aircraft resonances and reflections between simulated lightning columns and aircraft is shown in Figure 41. The feed and termination lines are connected at the selected attachment points. Wire size and proximity to ground are chosen to approximate the characteristic impedance of the lightning columns in the early time (300-600 ohms). The attached lines are terminated in that characteristic impedance at load and pulser to minimize reflection. The entire system is placed over a ground screen to minimize uncertain ground losses, keep propagation velocity near c_o, and provide a controlled low inductance return in later time. The aircraft may be blocked up or installed on a wood ramp to minimize gear ground capacitance. This approach is suitable for low to moderate level pulse drive as well as cw. The relatively large resistive impedance of this setup precludes high current testing, but, as previously mentioned, peak current is of secondary importance in relation to current derivative (rise rate).

70

0.25 INCH DIAMETER
CABLE LOADED
3Ω PER METER

HV
PULSER

GROUND SCREEN
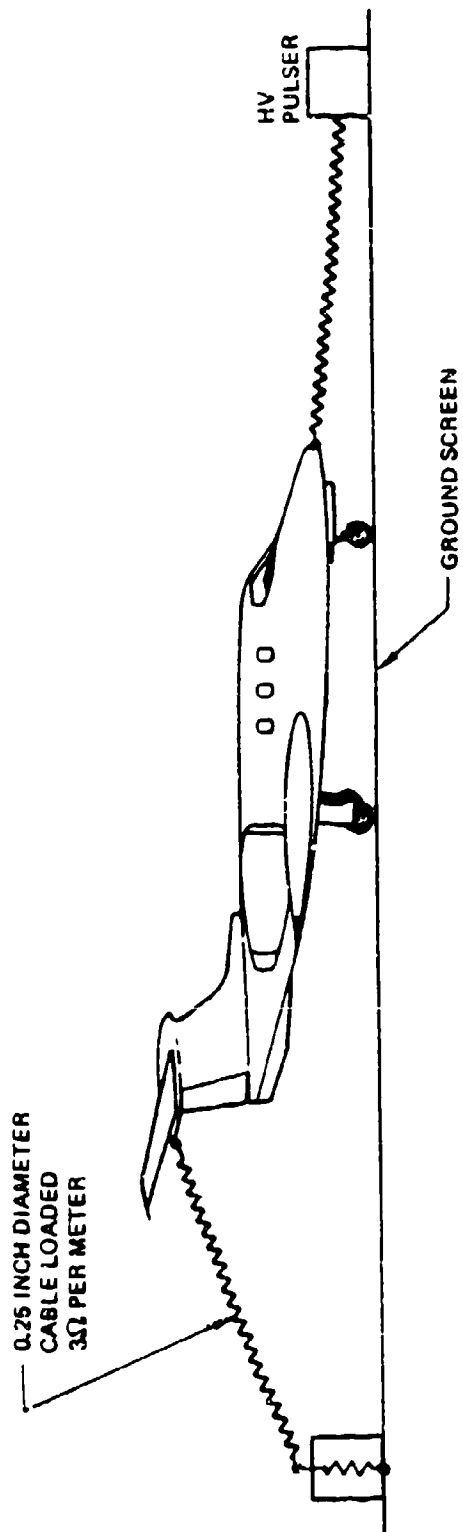
Figure 41. Recommended ground test configuration.

APPENDIX

INTERNAL TRAFFIC MODEL BLOCK DESCRIPTIONS

AA,BB   Distributed magnetic field source blocks for conductors
running along the rear spar of the right wing

AFTBLK   Tail field mill bundle and test wires running from the aft
equipment bay into the tail cone

AFTEST   Aft belly field mill bundle and test wires running in aft
equipment bay

AFTLOAD   Equivalent circuit load for aft field mill bundle and test
wires in aft equipment bay

BOALOAD   Equivalent circuit load for right wing field mill bundle
at tip of right wing

CABLOAD   Bulk load cabin termination for right wing Lear bundle

CABRUN   Bundle of right wing, left wing, tail, and aft belly field
mill bundles and test wires running inside the cabin

CBPANEL   Copilots dc circuit breaker panel equivalent circuit

CONTBOX   Copilots experimenters power system switchbox equivalent
circuit

CONTRUN   Experimenters power system control cable running in the aft
equipment bay

CONDSEC   Tail field mill bundle and test wires running inside the
protective conduit inside the tail

CONDUIT   Outside model of the conduit in the tail

DCFEED   Main dc power feeders from the generator control panel -
               dc bus system in the aft equipment bay to the copilots
               circuit breaker panel

ENDWING   The continuation of the right wing Lear bundle to its
               termination at the end of the wing

EXPCON   Experimenters power system control relay box equivalent circuit

EXPPWR   Experimenters power system control cable running inside cabin
               from the windows to the copilots control switch box

EXPRUN   DC power cable connecting the generator control panel to the
               experimenters power relay box

EXTPOW   DC power cable connecting the ground power unit connector to
               the generator control panel

FWDLOAD   Equivalent circuits for the dc loads on the copilots circuit
               breaker panel

GENCON   Generator control panel - dc bus system equivalent circuit

GPU   Ground power unit Norton equivalent circuit

HHBUND   Aft belly and tail field mill bundles and test wires and
               experimenters power control bundle running in the aft
               equipment bay

HHSOURCE   Mutual coupling source from ground power unit cable to
               aft field mill bundle and test wires

I"STLOD   Bulk load for the Lear sensor cables from the tail
               terminating in the cabin

INN   Equivalent load for experimenters power inverters

INVRUN   Power cables connecting the experimenters control relay
               box to experimenters power inverters

LWLOAD   Equivalent circuit loads for left wing field mill bundles
               and test wires

LWTEST   Left wing field mill bundle and test wires running inside
               left wing box

RWBA, RWBB,   Right wing test wires and Lear bundle running along rear
RWBC   spar of right wing

RWBOX   Right wing field mill bundle running inside right wing box

RWLOAD   Equivalent circuit termination for right wing test wires
               and bulk termination for right wing Lear bundle

SENSBND   Lear tail sensor cables running from the tail cone to the
               forward cabin

SHNTLOD   Bulk load for miscellaneous cables running behind the test
               equipment rack in the cabin

TESTBAY   Equivalent circuit terminations for right and left wing,
               tail, and aft belly field mill bundles and test wires at
               the equipment test rack in the cabin

TESTBND   Right and left wing, tail, and aft belly field mill bundles
                 and test wire cable section running from the test equipment
                 bay to the windows

TLOAD   Equivalent circuit load for the tail field mill bundle and
                 test wires at the top of the tail

TOLOAD   DC power cables running from copilots circuit breaker panel
                 to dc loads

TOPTAIL   Tail field mill bundle and test wires from the top of the
                 tail conduit to the tail termination

WINDOW   Electric and magnetic field source coupling from the window
                 aperture

WWBUND   Right wing field mill bundle and test wires running through
                 the wheel well

WWCAB   Right wing Lear bundle running through the wheel well into
                 the cabin

REFERENCES

1. DNA EMP Awareness Course Notes, DNA 2772T, Defense Nuclear Agency, August 1971.

2. H. Kaden, Wirbelstrome Und Schirmung in der Nachrichtentechnik, Springer-Verlag, Berlin, 1959.

3. Special Joint Issue on the Nuclear Electromagnetic Pulse, IEEE Transactions on Antennas and Propagation, Vol. AP-26, No. 1, January 1978.

4. R. F. Harrington, Field Computation by Moment Methods, MacMillan, New York, 1968.

5. W. L. Curtis, Computer Code "WIRANT," Boeing Document.

6. F. A. Fisher and J. A. Plumer, Lightning Protection of Aircraft, NASA Reference Publication 1008, October 1977.

7. D. F. Strawe, Analysis of Uniform Multiwire Transmission Lines, Boeing Document D2-26088-1, October 1972.

8. E. F. Vance and H. Chang, Shielding Effectiveness of Braided Wire Shields, SRI Technical Memorandum 16, November 1971.

9. A. C. Mong, A Frequency Domain Network Analysis Code - Users Guide, DNA Contract No. DNA 001-75-C-0049, April 1975.

10. PRESTO Digital Computer Code Users Guide, Volume 6, Modeling Library, D180-19028-3, Boeing Aerospace Company, Seattle, Washington, Contract DNA 001-75-C-0049, June 1976.

11. V. K. Jones and T. P. Higgins, Survivability/Vulnerability Safety Margin Assessment, D180-18163-14, Boeing Aerospace Company, Seattle, Washington, Contract DNA 001-75-C 0049, September 1975

12. PRESTO Digital Computer Code Users Guide, Volume 4, CIRCUS-11, Final Report, Defense Nuclear Agency, Contract DNA 001-75-C-0225, December 1975.

13. D. C. Wunsch and R. R. Bell, "Determination of Threshold Failure Levels of Semiconductor Diodes and Transistors Due to Pulse Voltages," IEEE Transactions on Nuclear Science, Vol. NS-15, No. 6, December 1968.

14. E. F. Vance, Prediction of Transients in Buried Shielded Cables, SRI Technical Report, March 1973.

15. Electromagnetic-Pulse Handbook for Electric Power Systems, Stanford Research Institute, 4 February 1975, Contract DNA 001-73-C-0238.

REFERENCES (Continued)

16. N. Cianos and E. T. Pierce, A Ground-Lightning Environment for Engineering Usage, SRI Technical Report 1, August 1972.

17. Lightning Source Model Development Program, D180-22936-1, Boeing Aerospace Company, Seattle, Washington, January 1978.

18. Single-Line Modeling Versus Multi-Conductor Modeling, M. L. Vincent and M. R. Borden, Boeing Aerospace Company, Seattle, Washington.